

Vessel motion prediction for Pioneering Spirit in shallow water

Quantification and reduction of uncertainty

F. van Vuuren



Vessel motion prediction for Pioneering Spirit in shallow water

Quantification and reduction of uncertainty

by

F. van Vuuren

to obtain the degree of Master of Science
at the Delft University of Technology,
to be defended publicly on Thursday Februari 22, 2018 at 14:00

Student number:	4159802	
Master program:	Offshore and Dredging Engineering	
Project duration:	April, 2017 – Februari 2018	
Chairman thesis committee:	Dr. Ir. A.P. van't Veer,	TU Delft
Supervisors:	Dr. Ing. S. Schreier	TU Delft
	Dr. Ir. N. Mallon	Allseas
	Ir. S. de Groot	Allseas

This thesis is confidential and cannot be made public until Februari 2020

Preface

With the completion of this thesis, my time as a student is coming to an end. The time has come to start a new chapter in my life, and I would like to say thanks.

I would like to thank my daily supervisors at Allseas, Niels Mallon and Sytske de Groot, for their help during the process, reading every part of my thesis and providing very helpful feedback and ideas. I would like to thank all other colleagues at Allseas for helping me with all kinds of questions I had, and also for the nice lunch breaks and vrijdagmiddagborrels. Furthermore I would like to thank Sebastian Schreier for being my daily supervisor and professor Riaan van't Veer for being the chairman of my committee. Both have helped me a lot by giving constructive feedback.

Furthermore, I would like to thank my parents for their support through all my years of study. I would like to thank my friends with whom i have studied long days at the university during my master. A special thanks goes to my girlfriend Melissa for supporting me and listening to me when I was talking about how interesting my project was, as well as motivating me in times I needed it.

Frits van Vuuren,
Delft, Februari 2017

Abstract

The *Pioneering Spirit* is a heavy lift vessel that can lift offshore platforms in a single lift. Due to the waves, the vessel moves with respect to the platform. To make sure the vessel does not hit the platform, a motion compensation system is installed on the *Pioneering Spirit*. The maximum allowable vessel motions during the operation are restricted by the capacity of the motion compensation system, see figure 1 Comparison of the predicted motions with measurements have shown good comparison for the deep water situation. It was found that prediction of the vessel motions in shallow water does not agree with the measured motions.

Therefore the prediction of the vessel motions in shallow water is investigated, to find out how do predicted vessel motions compare to measured motions. The goal is to quantify and reduce the uncertainty in vessel motion prediction in shallow water. First the calculation method of comparing the predictions to measurements was investigated and validated. The wave spectrum and as well as the Response Amplitude Operator (RAO) are available in 2D, The vessel response is available as a time series. To compare the predictions to measurements, both prediction and measurement are translated to a 1D response. For the prediction, first the 2D response is calculated, which is then added over all wave directions to get the 1D response. The measured time series of the vessel motions are translated to a 1D frequency domain response using the Fast Fourier Transform (FFT). The comparison of the 1D response spectra is done by comparing Significant Double Amplitude (SDA) and peak period T_p .

Comparison of the peak period has a relatively large error, with errors exceeding 0.5 s for most of the comparison for heave, roll and pitch. Looking at the SDA, the heave motions are underestimated for most of the time for low amplitudes. As the amplitudes increase, there is a spreading of the predicted motions above and below the measured values. Taking into account the motions with at least 0.4 m measured heave, the SDA is within 10 cm from the measured motions for 25% of the measurements. For the roll, the motions were under-predicted for larger motions, being at an incoming peak wave direction between than 220 and 260 degrees. The heave motions at the location of the topside lift system are dominated by the contribution of the pitch motions. The motions in shallow water are not accurately predicted in most cases, with a deviation from the heave at the sensor location by more than 10 cm. The response deviates above and below the measured motions. A possible explanation for the overestimation is the cushioning and sticking effect due to the presence of the seabed, this needs to be further investigated. The prediction of the peak period is limited by the precision of the buoy data. In order to do a good comparison for the peak period, the precision of the wave spectrum should be increased. This can be done by fitting the measured spectrum, or by using buoy data which has a smaller frequency step.



Figure 1: Heave motion at the location of topside lift system

List of Symbols

The next list describes the symbols used throughout this thesis

λ	Wave length
ρ	Density
ζ	motion in one of the six degrees of freedom or the wave elevation
$F_{diffraction}$	Diffraction force, force that occurs due to the presence of a vessel
$F_{Froude-Krilov}$	The wave force caused by incoming waves, also known as the Froude-Krilov force
$F_{hydrostatic}$	Hydrostatic force, the force due to the buoyancy of the vessel
H_{m0}	Significant wave height
m	Mass
p	Pressure
u	velocity in x-direction
v	velocity in y-direction
w	velocity in z-direction
ω	Frequency
Φ	Potential function
ϕ	Roll
ψ	Yaw
θ	Pitch
ε	Phase shift
a	Added mass
B	Beam of the vessel
b	potential damping
c	restoring coefficient
g	Gravitational acceleration
h	Water depth
k	Wave number
$S(\omega, \theta)$	2D wave spectrum or 2D response spectrum
T	Draught of the vessel
t	Time
T_p	Peak period
x	Surge
y	Sway
z	Heave

Glossary

CRP	Central Reference Point
FFT	Fast Fourier Transform
MRU	Motion Reference Unit
RAO	Response Amplitude Operator
SDA	Significant Double Amplitude
UKC	Under Keel Clearance

Contents

Preface	iii
Abstract	v
1 Introduction	1
1.1 Problem description	1
1.2 Objective	1
1.3 Research questions	2
1.4 Available data	2
1.5 Thesis structure	2
2 Previous Work	3
2.1 Linear Wave Theory	3
2.2 Non-linear effects	4
2.3 Viscous damping	4
2.4 Conclusions from literature	9
3 Theoretical Background	11
3.1 Potential Theory	11
3.2 Equation of Motion	12
3.3 Froude-Krilov force	12
3.4 Diffraction force	13
3.5 Radiation force	13
3.6 Hydrostatic force	13
3.7 Limitations hydrodynamic software package	14
3.8 Sensitivity of response to added mass and damping	14
4 The Motion Response Spectrum	17
4.1 Predicted Response Spectrum	17
4.2 Measured Response Spectrum	18
4.3 Comparing Spectra	19
5 Verification	23
5.1 Preliminary check	23
5.2 Comparing time domain to frequency domain	23
5.3 Sensitivity Analysis	26
5.4 Conclusions	29
6 Analysis of input data	31
6.1 Available data	31
6.2 2D wave spectrum	32
6.3 2D RAO	36
6.4 Time Series Measured	41
6.5 Validation rigid body motions	42
7 Test Results	45
7.1 Definition of good comparison	46
7.2 Help for reading figures	46
7.3 Results Offshore Acceptancy Test 1	46

8 Discussion of Results	57
8.1 Contribution of heave at CRP, roll and pitch to predicted heave.	58
8.2 Influence of motion amplitude on quality of prediction.	60
8.3 Prediction for different water depths	64
8.4 peak in roll motion	66
!	
9 Conclusions and Recommendations	69
A Fast Fourier Transform	73
Bibliography	75

Introduction

1.1. Problem description

The *Pioneering Spirit* is a heavy lift vessel that can lift offshore platforms in a single lift. Figure 1.1 shows the vessel just after lifting a platform from a jacket. Due to the waves, the vessel moves with respect to the platform. To be able to connect the lift points to the platform, a motion compensation system is installed on the *Pioneering Spirit*, to compensate the vessel motions in x, y and z direction. The maximum allowable vessel motions during the operation are restricted by the capacity of the motion compensation system. If the motions are too large, the system is no longer able to compensate the motions, as the system has reached its maximum stroke. Operation beyond its maximum stroke could lead to dangerous situations as the topside might hit its foundation after being lifted. These collisions should be prevented, and one wants to know in advance that motion limits are not exceeded during the total operation time of 12 to 48 hours. It is thus important to be able to predict motions based on weather forecasts. The vessel motions depend on the wave field, the loading condition and the vessel characteristics. Motion prediction becomes more complicated in shallow water, where the seabed has an influence on how the vessel behaves. The *Pioneering Spirit* has done some offshore trials and removed the Yme and Brent Delta Platforms. During these operations, vessel motion measurements have been carried out. Comparison of the predicted motions with measurements have shown good comparison for the deep water situation. In shallow water, the measured response deviates from the predicted one. This has been observed during offshore trials, which took place in the K-13 field in the North Sea from the 10th to the 16th of August 2016, in a water depth of 27 m with a draught of 20 m. A wave buoy was deployed in free water close to the *Pioneering Spirit*. This wave spectrum is used to predict the vessel motions at the lift point in the slot of the vessel.



Figure 1.1: Artist impression of *Pioneering Spirit* just after lifting a platform from a jacket, source: Allseas.com, 2017

1.2. Objective

The objective of this thesis is defined as follows:

"Quantification and reduction of uncertainty in vessel motion prediction - with special focus on shallow water."

This thesis aims to quantify and explain the difference between vessel motion measurements and predictions based on Response Amplitude Operator (RAO) and wave spectrum.

1.3. Research questions

To quantify and reduce the uncertainty of the vessel motion prediction, the following questions need to be answered:

- How do predicted vessel motions based on a measured wave spectrum compare to measured motions in shallow water?
- Vessel motion prediction in general
 - How do shallow water, small keel clearances and vessel shape influence the equation of motion?
 - What is the sensitivity of the individual effects towards the total response?
- On the current approach:
 - What steps are taken to predict the vessel motions?
 - Which effects are taken into account in the current approach?
 - Which effects are not taken into account in the current approach?
 - What is the validity range of the current approach?
 - How large is the uncertainty in the current approach?
 - Which effects need to be adjusted/added to obtain a result that shows better comparison with the real world situation?

1.4. Available data

For the comparison of predictions with measurements, data is available from the first offshore trials of the *Pioneering Spirit*, called OAT1, with a duration of approximately one week. The significant wave height is ranging between 1 and 3 m, and the peak period of the wave spectrum is ranging from 5 to 11 s. The incoming wave direction varies over time, both due to change in heading and change in peak direction of the wave spectrum.

1.5. Thesis structure

In order to answer the research questions, the structure of this thesis is as follows: First, chapter 2 discusses the previous work on vessel motion prediction in shallow water. Next, chapter 3 gives the theoretical background that is used in predicting the vessel motions. Chapter 4 explains how the response spectrum is calculated from the vessel specifics and the wave spectrum. Chapter 5 describes the verification of the calculation method. In chapter 6 the input data, which is used for the calculations, is analysed. It shows how the data is obtained and all processing that is needed before the calculations can be executed. Chapter 7 gives the results of the calculations and measurements, which are discussed in chapter 8 and from these the conclusions are drawn and recommendations are given in chapter 9.

2

Previous Work

A lot of research has been done on the behaviour of vessels in shallow water. In this chapter an overview is given from the previous work and the relevant information is summarized in the conclusion.

2.1. Linear Wave Theory

In linear wave theory, the ship motions in shallow water as a response to incident waves are affected in two ways[1]:

- The incoming wave is affected by the presence of the seabed. This causes a difference with respect to the deep water situation, where the presence of the seabed does not influence the wave.
- The presence of the seabed influences the hydrodynamic coefficients (added mass and potential damping) of the vessel.

Shallow water can be defined in different ways. A wave in shallow water behaves different compared to a wave in deep water. In linear wave theory, the ratio of water depth h over wave length λ determines whether a wave is a deep water, intermediate water, or shallow water wave. Figure 2.1 shows the wave height and water depth. For $h/\lambda > 0.5$, the waves are not influenced by the sea floor and are called deep water waves or short waves. For $h/\lambda < 0.05$ the waves are called shallow water waves or long waves. At the ratio between 0.5 and 0.05, the waves are called intermediate waves [2]. The different types of wave cause a different incoming wave force. The water is said to be shallow with regard to the vessel for a depth over draught ratio of $h/T < 7$, see figure 2.2. In which h is the water depth and T is the draught of the vessel [3]. Linear wave theory neglects the non-linear effects, these can however influence the motions significantly, and are discussed in the next section.

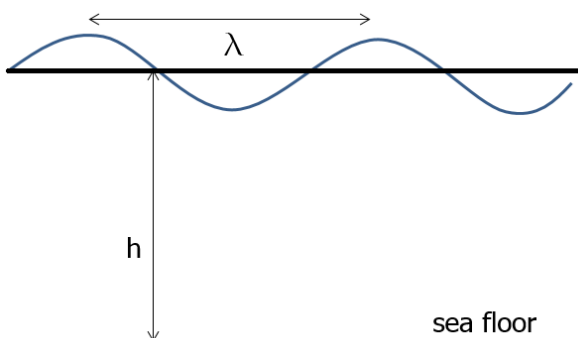


Figure 2.1: Definition of water depth h and wave length λ .

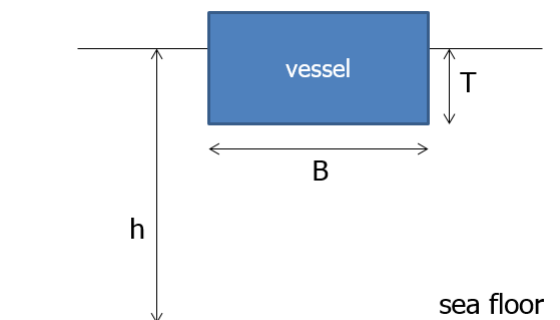


Figure 2.2: Definition of water depth h , and the vessel beam B and draught T

2.2. Non-linear effects

Linear wave theory does not take into account the non-linear effects, like cushioning and sticking. These non-linear effects can have a significant influence on the waves and the vessel motions [4].

Cushioning and Sticking

As the vessel is in the proximity of the seabed and moving down, the resistance to the vertical downward movement is higher than in deep water. This is because the water particles can move out less easily from underneath the vessel. This is called the cushioning effect. Opposite to the cushioning effect, the sticking effect makes it harder for the vessel to accelerate upward in shallow water. Just as the water particles cannot move easily from underneath the vessel, they cannot easily move back underneath the vessel either. This is called the sticking effect. Both the cushioning and sticking effect are a consequence of the change in added mass. As the under keel clearance reduces, the added mass increases. The added mass for a heaving motion in shallow water thus changes over time. This is not taken into account in the frequency domain. To account for the time varying added mass the response needs to be calculated in the time domain, it cannot be taken into account in the frequency domain. Peters and Huijsmans [4] investigated the effect of shallow water on a forced oscillation test for a truncated cylinder. Looking at how to compare this to the *Pioneering Spirit*, the water depth over draught h/T is 1.2 for the experiment, and for the *Pioneering Spirit* 1.35. The ratio of the vessel heave motion amplitude over under keel clearance z/UKC was set to 0.5. For *Pioneering Spirit* the ζ_3/UKC is a lot smaller, around 0.15. The results of including the cushioning and sticking effect, are shown in figure 2.3. In this figure it can be seen that linear motions do not take into account the cushioning and sticking effect. These effect become stronger as the under keel clearance becomes smaller. As the cylinder moves down, the cushioning effect is observed as the water is squeezed out of the gap underneath the cylinder. When the cylinder starts moving up, the sticking effect occurs. Compared to the deep water situation, more force is required to accelerate the cylinder up or down.

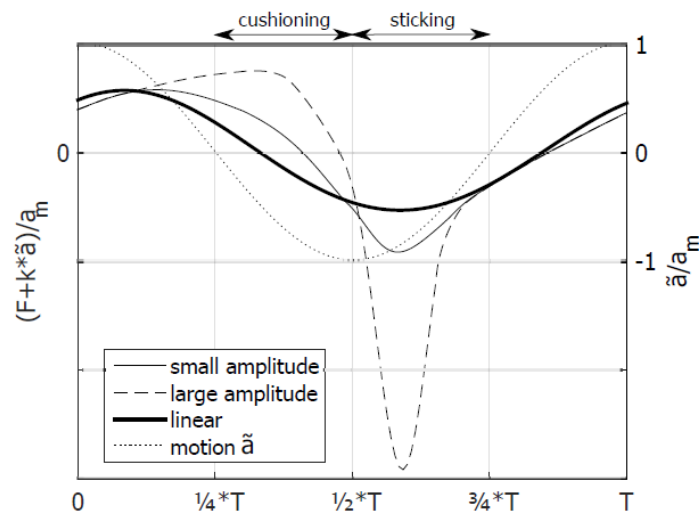


Figure 2.3: Trend of non-linear load for a forced oscillation of a cylinder due to squeeze flow. F is the hydrodynamic load, \ddot{a} is the time dependent motion, a_m is the motion amplitude, k is the restoring stiffness and T is the harmonic period. It can be seen that more force is required for the forced oscillation as the amplitude of the motion increases. Source: Peters and Huijsmans (2017)[4]

2.3. Viscous damping

Damping of the vessel motion is caused by the generation of waves (the potential damping) and by viscous effects. Viscous effects include skin friction and vortices among others. These effects are generally neglected as they are small compared to the contribution of the potential damping. However, for the roll damping, the potential damping can be relatively small. This means that the contribution of the viscous effects can become significant [2]. Figure 2.4 shows the influence of the breadth over draught ratio of a vessel on the potential wave damping. From the figure, it can be seen that the wave damping is smallest for a B/T ratio of about 2.5.

For such ratios, the contribution of viscous damping is relatively high. However, for the *Pioneering Spirit*, the ratio B/T has a value of around 6. For such vessel shapes, it can be seen from the figure that the potential wave damping is relatively large. It is thus expected that the contributions of viscous damping are smaller for *Pioneering Spirit* than for 'regular' vessels, which have a lower B/T ratio. Relevant papers about shallow water behaviour of vessels are summarized below. For every paper, three questions are answered: what has been investigated, why has it been investigated and what can be concluded.

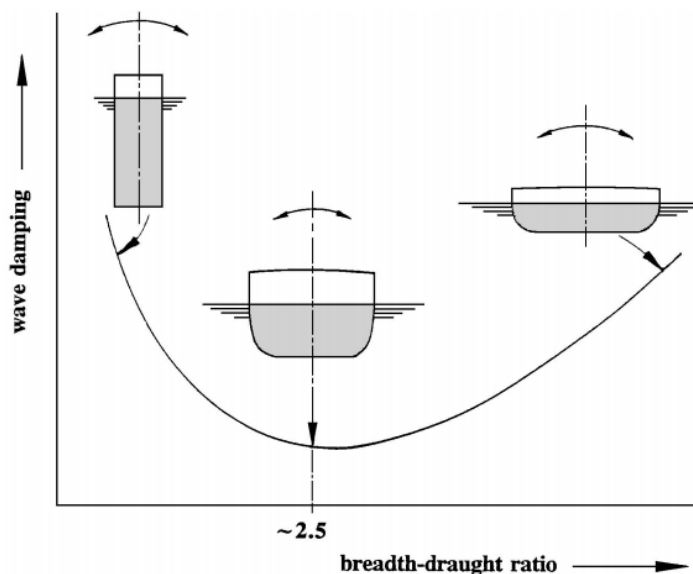


Figure 2.4: Influence of beam over draught ratio (B/T) on the wave (or potential) damping. For a B/T ratio of 2.5, the wave damping is very small, which means the contribution of viscous damping can be significant. For *Pioneering Spirit*, B/T is around 6, which means the wave damping is relatively large, and the contribution of viscous damping is expected to be smaller compared to vessels with lower B/T ratios. Source:[2]

Simplified formulas of heave added mass coefficients at high frequency for various two-dimensional bodies in a finite water depth

What has been investigated?

Koo and Kim [3] developed simplified formula for added mass coefficients of a two-dimensional floating body, moving vertical in a finite water depth. Use is made of linear wave theory.

Why has it been investigated?

Current calculation methods for heave added mass in finite water depth are time consuming and expensive.

What can be concluded?

At high frequencies, the added mass converges to a constant value and is no longer dependent on the frequency.

The result from the simplified formula is compared to the results from a Numerical Wave Tank (NWT) technique. The NWT calculations are based on linear wave theory. For high frequency, the added mass goes to a constant value. The added mass at high frequency calculated from the NWT is used as a basis, to which a correction factor is applied to account for lower frequencies and the presence of the sea floor. The prediction of added mass at high frequencies for various geometric conditions give good results. The test is executed for 2 dimensional shapes moving up and down. When going to a smaller water depth, the added mass of a rectangular shape increases more than for a circular shape. This is because the effective wetted surface is larger for a rectangular shape than for a circular shape. The formulas are also valid for various wave frequencies, until the normalised frequency ($\omega\sqrt{B/2g}$) becomes greater than 1.0. Where ω is the wave frequency, B is the beam and g is the gravitational acceleration. For high B/T ratios (B is the beam, T is the draught of the

vessel), the simple formulas deviate more from the NWT model. The formulas hold for a B/T ratio up to 3, which is typical for normal vessels, and can be used for a quick analysis of the added mass in shallow water region.

Challenges with ship model tests in shallow water waves

What has been investigated?

Ruiz et al. [5] looked into the challenges encountered in shallow water model testing and how can they be coped with.

Why has it been investigated?

During previous tests, challenges with modelling were experienced in shallow water, relating to the ship motions, the propagation of the waves in shallow water and the wave behaviour in shallow water. To the authors best knowledge, no guidelines for model tests in shallow water waves have been established.

What can be concluded?

For model tests, it is assumed that bottom interaction can be neglected for a water depth h over mean draught T_m of $h/T_m < 4$. and for waves as $kh < 1/10$. in which k is the wave number. In shallow water, additional effect compared to deep water are present. Waves develop in a non-linear manner which is dependent on their period and amplitude. Depending on the under keel clearance the ship is facing large hydrodynamic forces. Shallow water waves behave different along the tank, energy dissipation is observed as they travel along the tank. There is however a range in the tank where the waves can be considered stable. In this study, the vessels have a forward speed. Bottom touch events become a significant problem for less than 20% under keel clearance. If wave height and ship motions are small, the side-wall interaction effect on heave and pitch motions can be neglected. Difference is observed in the interaction effect for following and head waves. In following waves, the interaction is stronger (vessel is moving forward). To the authors best knowledge, guidelines for model tests in shallow water waves have not been established yet.

Bilge keel damping from in-field motion measurements

What has been investigated?

In this article by Voogt [6], the actual damping for an FPSO is measured in the real world situation. The measurements are compared to the damping estimated from a model.

Why has it been investigated?

Roll damping in models is often conservative, meaning the roll motion is over estimated.

What can be concluded?

FPSO heading appears to be primarily dominated by current, while wind is playing a secondary role. this is against established norms. Local sea and swell have little influence on the vessel heading. The roll RAO can be assumed independent of draught for this FPSO. Model scale damping in calm water is conservative, compared to real data from this FPSO, due to the conservatism built into the roll damping estimate.

Comparison of AQWA, GL Rankine, MOSES, OCTOPUS PDSTRIP and WAMIT with model test results for cargo ship wave-induced motions in shallow water

What has been investigated?

Gourlay et al. [7] did a benchmark study concerning the wave-induced ship motions in shallow water (a water depth over draught ratio of 1.2), predicted with commercially available codes AQWA, GL Rankine, MOSES, OCTOPUS, PDStrip and WAMIT. The heave, pitch and roll motions are compared.

Why has it been investigated?

To assess the suitability of each code for zero-speed applications as well as forward speed applications. So far, publications on the bench marking of various numerical models in shallow water have not been available in open literature.

What can be concluded?

Heave in beam waves is predicted well by most codes. In head waves at zero speed, the heave RAO peaks and troughs generally follow the wave induced heave force. Heave damping may be over predicted at resonance frequency in head waves. In beam waves, this over prediction is not seen and the test results compare well with the model tests. Comparison of RAOs for different software packages, shows small deviations. The RAOs look alike but are not exactly the same. The bench marking in general shows a good result, wave induced motions are not over or under predicted in general, but deviate above and below the model test results. It is concluded that motion response spectra and spectral characteristics of ship motions in irregular waves is reasonably well predicted by combining transfer functions of ship motions with energy of irregular seaways. However, due to the limiting width of the available towing tanks, the results only show limited range of ship speed and wave direction combinations. It was found that for zero forward speed as well as for forward speed, the vessel motion predictions generally compared well with the model test results. An exception is the roll amplitude. This could not be compared directly because viscous effects play an important role on the roll damping. The various software packages use different approaches to handle this. The roll damping was not compared in this study.

Effect of spectral shape uncertainty in the short-term wave-induced ship responses**What has been investigated?**

Soares [8] looked into the sources of fundamental, statistical and model uncertainty in the spectral description of wave elevation, for a stationary sea. The uncertainties that occur in the response variance due to the uncertainties in the spectrum shape are quantified.

Why has it been investigated?

To quantify the uncertainty in the response variance due to the uncertainty in spectrum shape and for a verification of the methods that are used.

What can be concluded?

The spectral approach is accepted to be the correct way to calculate short term ship responses to wave actions. The measurement of a wave spectrum is subject to both systematic and random error. Separation can be made between statistical and fundamental uncertainties. Statistical uncertainties are the variability of each parameter around its mean value. Fundamental uncertainties represent the probability of occurrence of the various spectral shapes. With a decrease in the mean value of the response, the standard deviation increases. The method for calculation of the response for the tankers in a wide range of ship lengths which are tested here, can vary between 20% overestimation to 30% under estimation, depending on the specific case. For ships larger than 300 m in length, the response becomes unconservative for sea states with a significant wave height less than 4 to 6 meters.

Full-scale unsteady RANS simulations of vertical ship motions in shallow water

What has been investigated?

Tezdogan et al. [9] did a numerical study on the behaviour of vessels in shallow water, using a commercial Unsteady Reynolds–Averaged Navier–Stokes URANS solver. First, characteristics of a shallow water wave were investigated by doing simulations. Next, a case study with a full-scale tanker has been done to predict heave and pitch responses to head waves at zero speed, for head waves at different water depths. The results are compared with other studies from literature and 3D-potential theory.

Why has it been investigated?

Literature on shallow water often misses the validation with real world measurements.

What was the conclusion?

Transfer functions obtained from the CFD method showed a fairly good agreement with experimental data for a water depth over draught ratio $h/T = 4.365$. However, the difference became larger as the vessel came closer to the seabed. 3D-panel methods over-predict heave and pitch transfer functions for a $h/T = 1.2$. This can however also be caused by the coarse panel generation in the 3D panel method. It is stated that recently developed 3D potential theories based on for example the Rankine source panel may give better results. Overall, the URANS method gave better results than the potential flow theory used in this paper, especially for pitch motions. If the water depth decreases, the peak in the pitch transfer function shifts to lower frequencies.

Effect of shallow and narrow water on added mass of cylinders with various cross-sectional shapes

What has been investigated?

Zhou et al. [10] analysed numerically the effects of shallow and narrow water on the added mass of a cylinder for sway, heave and roll.

Why has it been investigated?

The contribution of the added mass is significant in the motions of a cylinder. For the deep water situation, a lot of literature is present on the added mass. For the shallow water situation there is less literature available.

What was the conclusion?

The results are compared to previous literature, and the results agree well. In shallow water and in narrow water a significant increase in added mass can be observed. The shape of the cylinder has a large influence on the effect of shallow water. A circular, triangular and rectangular shape are compared, all for a range of draught over water depth. The shallow and narrow water effect are the strongest on the rectangular, shape, and weakest on the triangular shape.

Prediction of relative vertical motion between cargo and heavy transport vessel during offshore loading and discharge

What has been investigated?

In this paper, the prediction of relative vertical motion, dominated by the phenomenon squeeze flow, has been investigated by Peters and Huijsmans [4]. This effect is comparable for shallow water operations. The ratio of the vessel heave motion amplitude over under keel clearance z/UKC was set to 0.5.

Why has it been investigated?

Linear solutions that are used, do not take into account the non-linear effects, which are caused by the squeeze flow. This causes the predictions to be inaccurate in predicting relative vertical motions between the cargo and the heavy transport vessel (HTV).

What was the conclusion?

In linearized solutions, small motion amplitudes are assumed with respect to the characteristic dimensions of the flow problem. This assumption does not hold for squeeze flow. The added mass is found to have a strong dependence on the gap height. This dependence on the gap height gives a strong effect on the hydrodynamic load. In order to take the non-linear effect into account, the motion prediction requires a time domain approach, as in the frequency domain, the non-linearities cannot be accounted for.

2.4. Conclusions from literature

The following conclusions can be drawn from the literature that has been investigated in this chapter:

- Literature on shallow water has limited validation with real world experiments
- The RAOs for shallow water (a water depth over draught ratio of 1.2) calculated from different software packages show almost the same result. Calculation of the response with this given RAO gives results that compare well with model tests for heave roll and pitch, for head waves and beam waves.
- Most studies focus on 'normal' vessel shape: beam over draught ratio < 3 . Pioneering Spirit has a beam over draught ratio varying between 5 and 10.
- As the amplitude of the response decreases, the relative uncertainty in the response increases, therefore small vessel motions have a relatively high uncertainty.
- Going from deep to shallow water, the added mass increases significantly.
- Shallow water effect is stronger on rectangular shape than on circular shape and weakest on a triangular shape
- added mass changes depending on under keel clearance and depending on frequency. For small under keel clearance, the added mass changes significantly in time for a heaving motion. Starting from a water depth over draught ratio of 7, this effect occurs. The effect becomes stronger as the water depth decreases.

On potential theory:

- Spectral approach with potential theory gives good results in deep water
- For very small under keel clearances, CFD gives significant better results than potential theory
- In the frequency domain, the time-varying change in added mass is not accounted for
- Viscous forces are not accounted for in potential theory
- Viscous forces can be significant for an approaching seabed
- Viscous forces can be significant for the roll damping

3

Theoretical Background

A vessel can move in six degrees of freedom, this is shown in figure 3.1. To describe these motions, one should know how the vessel responds to waves. For this, different theories can be used. Potential theory is widely used. The assumptions and resulting motions are discussed in this chapter.

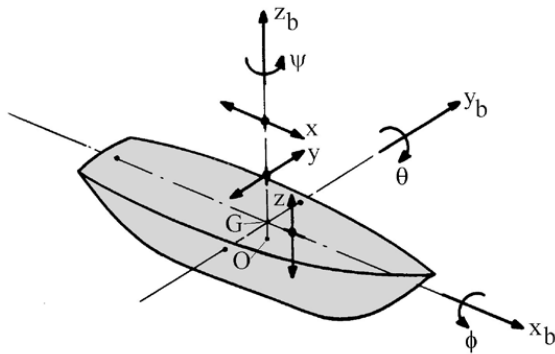


Figure 3.1: Six degrees of freedom for vessel motions

index	name	symbol
1	surge	x
2	sway	y
3	heave	z
4	roll	ϕ
5	pitch	θ
6	yaw	ψ

Table 3.1: The six degrees of freedom for vessel motions

3.1. Potential Theory

In Potential theory, the waves are assumed to move harmonic. The wave field is described as the sum of harmonic waves with each their own frequency and phase. The flow is assumed to be incompressible, irrotational and continuous. The following equation can be obtained, for this type of flow:

$$\frac{\partial u}{\partial x} + \frac{\partial v}{\partial y} + \frac{\partial w}{\partial z} = 0 \quad \text{continuity equation} \quad (3.1)$$

In which $[u,v,w]$ are the velocities in the $[x,y,z]$ directions. The potential function Φ is defined such that the velocity component in any chosen direction is the derivative of this potential function in that chosen direction. This leads to the following equation, also known as the Laplace equation:

$$\frac{\partial^2 \Phi}{\partial x^2} + \frac{\partial^2 \Phi}{\partial y^2} + \frac{\partial^2 \Phi}{\partial z^2} = 0 \quad (3.2)$$

In which Φ is a potential function. Since there is no friction within the potential flows being discussed here, energy is conserved along a streamline. Assuming steady flow, we can find the pressure from the Bernoulli equation:

$$p = \rho \frac{\partial \Phi}{\partial t} - \frac{1}{2} \rho (u^2 + v^2 + w^2) - \rho g z \quad (3.3)$$

In which p is the pressure, ρ is the density of the fluid and g is the gravitational acceleration. Ignoring the second order effects, the equation becomes:

$$p = \rho \frac{\partial \Phi}{\partial t} - \rho g z \quad (3.4)$$

In which the first term on the right hand side is the first order fluctuating pressure, and the second term is the hydrostatic pressure.

3.2. Equation of Motion

Different forces are acting on a vessel that is moving in the waves. The incoming wave force or Froude-Krilov force is the force that results from the pressure in a wave. The diffraction force is the force that occurs due to the presence of the vessel. The radiation force is the force caused by the movement of the vessel and the hydrostatic force is the force due to buoyancy. The equation of motion for a vessel in waves can be described based on Newton's second law as follows:

$$m\ddot{\zeta} = F_{Froude-Krilov} + F_{diffraction} + F_{radiation} + F_{hydrostatic} \quad (3.5)$$

In which ζ is the motion in one of the 3 directions, surge, sway and heave. The radiation and hydrostatic forces can be expressed in terms of added mass a , potential damping b and a stiffness term c . The equation can then be written as:

$$(m + a)\ddot{\zeta} + b\dot{\zeta} + c\zeta = F_{Froude-Krilov} + F_{diffraction} \quad (3.6)$$

For the roll pitch and yaw a similar equation can be written, where the mass and added mass become mass moments of inertia and with moments instead of forces. The response to irregular waves is based on linear theory, this means the superposition principle can be used. The wave forces and the motions are harmonic, and so the forces can be described in the form:

$$F = F_a \cos(\omega t + \varepsilon_{F, \zeta_{wave}}) \quad (3.7)$$

and the motions can be described in the form:

$$\zeta = \zeta_a \cos(\omega t + \varepsilon_{\zeta, \zeta_{wave}}) \quad (3.8)$$

in which ω is the frequency, $\varepsilon_{F, \zeta_{wave}}$ is the phase between the force and the wave, and $\varepsilon_{\zeta, \zeta_{wave}}$ is the phase between the vessel motion and the wave. The potential force can be calculated by using Green's theorem assuming sources over the body of the vessel S_0 . [2]

3.3. Froude-Krilov force

The incoming wave force, or Froude-Krilov force, is calculated assuming an undisturbed wave that causes pressures over the hull of the vessel. The pressure is calculated from the velocity potential. with the pressure integrated over the submerged area of the vessel, the wave force is found to be:

$$F_{Froude-Krilov} = \int \int_{S_0} (p \bar{n}) dS \quad (3.9)$$

similar for moments:

$$M_{Froude-Krilov} = \int \int_{S_0} p(\bar{r} \times \bar{n}) dS \quad (3.10)$$

In which S_0 is the average submerged area, p the pressure, \bar{n} is the unit vector pointing outwards from the hull and r is the distance from the rotation point. The incoming wave can also be written by means of a potential function, written in the form:

$$\Phi_{Froude-Krilov}(x, y, z, t) = \frac{\zeta_a g}{\omega} \frac{\cosh(k(h+z))}{\cosh(kh)} \sin(kx \cos \mu + ky \sin(\mu) - \omega t) \quad (3.11)$$

From this potential function, the first order fluctuating pressure can be calculated using formula 3.4

3.4. Diffraction force

The diffraction force is the force that occurs due to the presence of the vessel. Waves do not penetrate through the body but are reflected by it. This means the following boundary condition holds:

$$\frac{\partial \Phi_{Froude-Krilov}}{\partial n} + \frac{\partial \Phi_{diffraction}}{\partial n} = 0 \quad (3.12)$$

3.5. Radiation force

The radiation force is the force that occurs due to the motion of the vessel. This vessel motion causes dynamic forces in the surrounding fluids. In linear theory, it is assumed that the radiation force is proportional to the vessel motions. The radiation potential can be written as:

$$\Phi_{r,i} = \Phi_{ar,i} \cos(\omega t + \varepsilon_{\Phi_{r,i},\zeta_i} + \varepsilon_{\zeta_i,\zeta}) \quad (3.13)$$

Which can also be written in complex form as:

$$\Phi_{r,i} = \text{Re} \left[\Phi_{ar,i} e^{-i\varepsilon_{\Phi_{r,i},\zeta_i}} e^{-i\varepsilon_{\zeta_i,\zeta}} e^{-i\omega t} \right] = \text{Re} \left[\Phi_{ar,i} e^{-i\varepsilon_{\Phi_{r,i},\zeta}} e^{-i\omega t} \right] \quad (3.14)$$

In which $\Phi_{r,i}$ is the radiation potential in the i -th direction, $\varepsilon_{\Phi_{r,i},\zeta_i}$ is the phase angle of the radiation force in the i -th direction with the motion in the same direction. $\varepsilon_{\zeta_i,\zeta}$ is the phase angle between the motion ζ_i in the i -th direction and the wave elevation ζ . Similar to the incoming wave force, the radiation force is calculated by integration over the submerged area:

$$F_{radiation,i} = \int \int_S (p_{r,i} n_i) dS = \int \int_S \left(\rho \frac{\partial \Phi_{r,i}}{\partial t} n_i \right) dS \quad (3.15)$$

In which $p_{r,i}$ is the pressure due to radiation in the i -th direction and ρ is the density of the water. A common way of describing the radiation force is in terms of added mass and potential damping. The added mass is associated with the acceleration, and the potential damping is associated with the velocity. From equation 3.15, the added mass a and the potential damping b can be derived:

$$a_{ij} = \text{Re} \left[\int \int_S (-\rho \phi_{r,j} n_i) dS \right] \quad (3.16)$$

$$b_{ij} = \text{Im} \left[\int \int_S (-\rho \phi_{r,j} \omega n_i) dS \right] \quad (3.17)$$

Where a_{ij} and b_{ij} are the added mass and damping in the i -th direction due to motion in the j -th direction.

Added Mass

Added mass is the inertia added to the vessel because accelerating or decelerating the vessel requires moving (or deflecting) some volume of surrounding water as it moves through it. The added mass is dependent on the wave frequency. As the wave frequency increases, the added mass increases and converges to a constant value when the frequency goes to infinity [3].

Potential Damping

Potential damping is the damping that is introduced due to the vessel motions which creates waves. The radiation wave damping decreases for increasing frequency. It goes to zero as the frequency goes to infinity[3].

3.6. Hydrostatic force

The hydrostatic damping force is caused by the buoyancy, as the vessel moves down, the buoyancy force increases, this increase is described by a restoring component c_{ij} .

$$F_{hydrostatic,ij} = -c_{ij}\zeta \quad (3.18)$$

3.7. Limitations hydrodynamic software package

To calculate the RAOs, the hydrodynamic software package AQWA-LINE version 18.2 is used. In the calculation, the vessel is assumed to be symmetrical, and therefore only one half of the vessel is modelled, for incoming waves of 0 to 180 degrees. These results are mirrored to obtain the RAO from 0 to 360 degrees. This software has the following theoretical limitations [11]:

- The theory relates to a body or bodies which have zero or small forward speed. In the calculations in this thesis the vessel will not have forward speed so this will not cause problems.
- The motions are to a first order and hence must be of small amplitude
- The incident regular wave train must be of small amplitude compared to its length (i.e. small slope).
- The fluid is assumed inviscid, incompressible and the fluid flow irrotational
- All body motions are harmonic
- The forces and moments on a fixed body require only the diffraction problem to be solved
- No viscous damping is included within the analysis
- The added mass is calculated for the equilibrium position, it does not vary over time, while this may be the case in reality.

3.8. Sensitivity of response to added mass and damping

From previous work (see chapter 2), it was found that the proximity of the sea bed can cause a change in added mass and potential damping. To find how these changes affect the response at different frequencies, first the response is calculated for different frequencies using the general motion equation for a vessel moving in waves:

$$(m + a(\omega))\ddot{\zeta}_i + b(\omega)\dot{\zeta}_i + c\zeta_i = F_a \cos(\omega t) \quad (3.19)$$

In which ζ_i is the motion in the i -th direction, m is the mass, a is the added mass, b is the potential damping, c is the hydrostatic damping, this leads to a response amplitude of:

$$\zeta_{i,a} = \frac{F_a}{\sqrt{(c - \omega^2(m + a(\omega)))^2 + (b(\omega)\omega)^2}} \quad (3.20)$$

Where it should be noted that in reality, both a and b are a function of the frequency ω . For sake of simplicity, the added mass and damping are assumed constant for this sensitivity check. The response in equation 3.20 is dependent on the frequency. For very low frequencies, the terms that are multiplied by ω (the potential damping) and ω^2 (added mass) are very small. The motion is dominated by the restoring coefficient c . For the limit of $\omega = 0$ a change in added mass or potential damping does not influence the response. For intermediate frequencies, the restoring force c and $\omega^2 a$ cancel each other, this is the eigenfrequency of the system. At these intermediate frequencies, the potential damping is dominating the response. For very high frequencies, the added mass is dominating as it is multiplied by ω^2 , so the response is mostly dependent on the added mass for high frequencies. To correctly see the influence of over or under prediction of added mass and potential damping, different combinations are simulated. The results of the study are shown in figures 3.2-3.6.

Larger added mass

Figure 3.2 shows the influence of an increased added mass on the motion response. For the lower frequency, the response increases, while at higher frequency the response decreases. For high frequencies, the contribution of the added mass to the response increases, as it is multiplied by ω^2 .

Larger potential damping

A larger potential damping, leads to a response that is smaller for all frequencies. The effect is the strongest at intermediate frequencies, i.e. frequencies around the eigenfrequency of the system. This is because the restoring term and the added mass cancel each other at the eigenfrequency of the system. Next to the decrease in response amplitude the peak of the response slightly moves to the lower frequencies as can be seen in figure 3.3. As expected, for high frequencies, the response is hardly influenced by the potential damping.

larger added mass and larger potential damping

If both the added mass and potential damping are larger, the effect depends strongly on the combination of the change in added mass and the change in potential damping. In graph 3.4 the damping effect dominates, and the response is smaller for all frequencies. However, if we reduce the potential damping increment, a different situation occurs where lower frequencies have a larger response, while higher frequencies have a smaller response.

Smaller added mass, larger potential damping

See figure 3.5. For smaller added mass and larger potential damping, the result is smaller for intermediate frequencies, the higher frequencies give a larger output.

Larger added mass, smaller potential damping

For the intermediate frequencies, the response is larger, and for larger frequencies, the response is smaller. This is shown in figure 3.6.

Conclusion sensitivity study

Increased added mass causes an increase of the response in the lower frequency part, and a decrease in the higher frequency part. Increased potential damping causes a decrease in the response amplitude, this effect is the strongest around the resonance frequency. The increasing potential damping also causes (a small) shift of the peak frequency to the lower frequencies as is shown in 3.3. A different added mass or damping influences the motion response. In practice, this means that a wrongly estimated added mass or damping term, can cause a wrong motion prediction. See figure 3.2, if the black line represents the current estimate, and red is the line of the real world situation, it can be seen that for low frequencies, the response is underestimated, while the response at higher frequencies is overestimated. The response is dominated by the potential damping in the intermediate frequencies, and by the added mass for high frequencies.

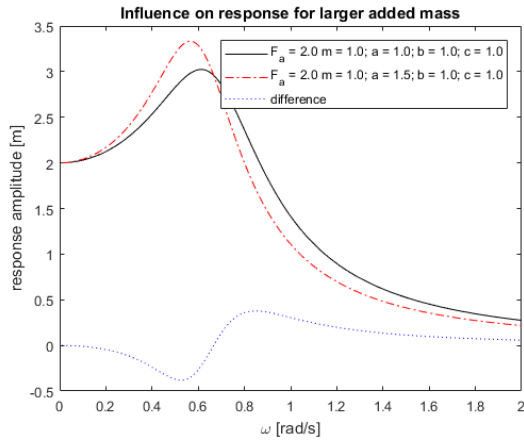


Figure 3.2: Influence on the response amplitude for larger added mass

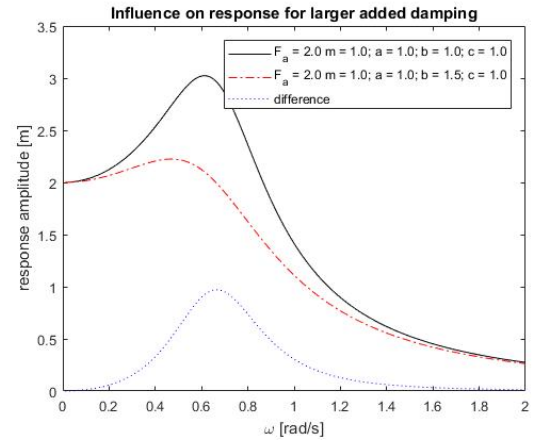


Figure 3.3: Influence on the response amplitude for larger potential damping

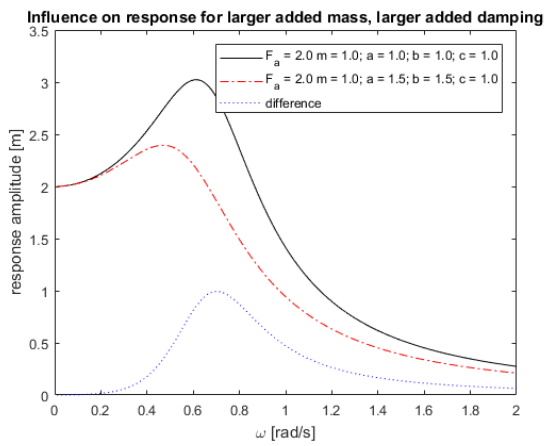


Figure 3.4: Influence on response amplitude for larger added mass and larger potential damping

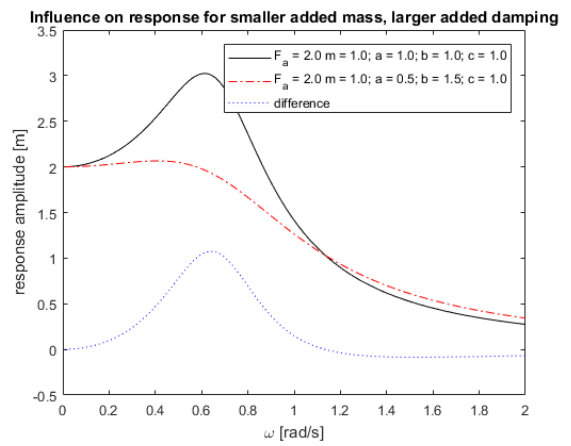


Figure 3.5: Influence on response amplitude for smaller added mass and larger potential damping

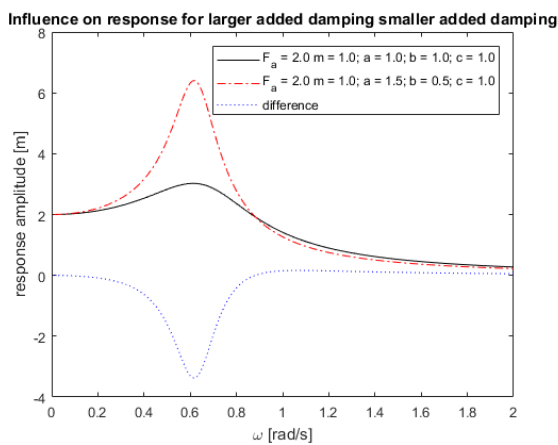


Figure 3.6: Influence on response amplitude for larger added mass and smaller potential damping

4

The Motion Response Spectrum

Comparison of predicted and measured vessel motions is only possible in the frequency domain, because the wave field is only available in the frequency domain. Prediction is done based on a wave spectrum in the frequency domain that was measured by a buoy. This buoy spectrum has no information about the phases of the waves. The measured vessel motions are available in the time domain. These time domain motions need to be converted to the frequency domain, in order to compare them to the predicted motions. This chapter will describe how the prediction is made based on a wave spectrum and RAO, and how to compare this to the measured vessel motions.

4.1. Predicted Response Spectrum

The response spectrum is predicted by using an RAO and a wave spectrum. The RAO is calculated by using the theory described in chapter 3. The wave spectrum is measured by a wave buoy. Once the RAO and wave spectrum are known, the response spectrum can be calculated. The wave spectrum $S_{\zeta}(\omega, \theta)$ and $RAO(\omega, \theta)$ are both given in 2D, which means they depend on both the frequency and the direction, as shown in figure 4.1. The RAO and wave spectrum do not necessarily have the same angular step. This means that before the response can be calculated, first the RAO and wave spectrum should have the same angular directions. The RAO is interpolated such that it has the same directions as the wave spectrum. Figure 4.1 shows the RAO and wave spectrum both with the same directional step. The direction $N=2$ is highlighted, and is shown in detail in figure 4.2. The calculation area in frequency direction is chosen for the area where both the RAO and wave spectrum are non-zero, because this will give a non-zero response, as can be seen in figure 4.2. The response is calculated per direction. First, the response is calculated for every direction and frequency separately. This results in the 2D response spectrum. Then the 2D response spectrum is transformed to a 1D response spectrum. This is necessary because the measured vessel motions to which the prediction will be compared, can only be transformed to a 1D spectrum. The response spectrum for the motion in (for example) the z -direction is defined as:

$$S_z(\omega, \theta) = S_{\zeta}(\omega, \theta)RAO^2(\omega, \theta) \quad (4.1)$$

In which $S_z(\omega, \theta)$ is the response spectrum for the z direction and $S_{\zeta}(\omega, \theta)$ is the wave spectrum. After the 2D response is obtained, it is transformed to a 1D response. The energy is summed over the directions. Figure 4.3 shows an example of a 2D heave response spectrum and the 1D heave response spectrum. In a 2D spectrum, the energy is divided over the frequencies and directions, in a 1D spectrum, the energy is divided only over the frequencies. The total energy in a 1D and a 2D spectrum remains the same. To arrive at the 1D spectrum, the following formula is applied (again for the example in the z -direction):

$$S_z(\omega) = \sum_1^N S_z(\omega_N, \theta) \quad (4.2)$$

In which $S_z(\omega)$ is the spectrum density in 1D, $S_z(\omega, \theta)$ is the 2D spectrum density, and N is the number of wave directions used in the 2D spectrum. The units for the 1D spectrum are [$m^2 s$] and the units for the 2D spectrum are [$m^2 s/rad$].

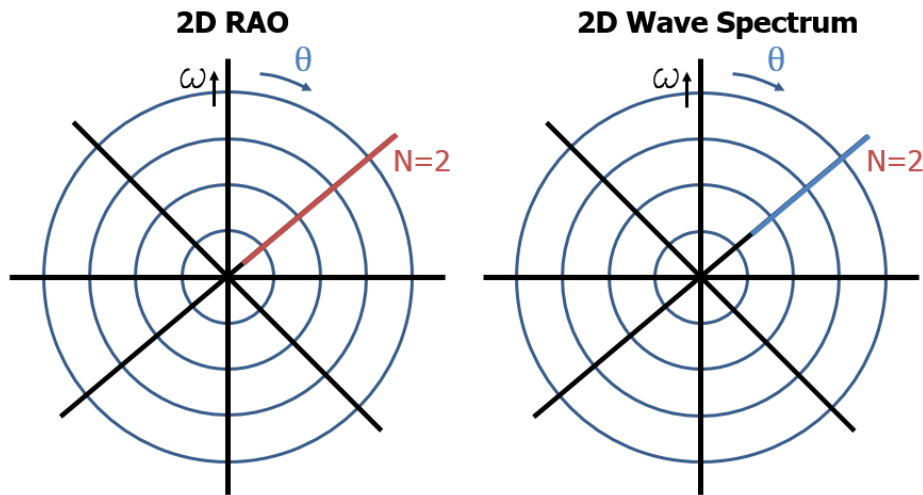


Figure 4.1: Top view of 2D wave spectrum and RAO. The response is calculated per direction, after which the response from all directions is added to get the final 1D response

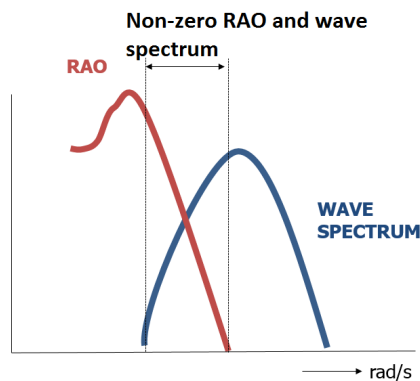


Figure 4.2: The RAO and wave spectrum for a given direction $N=2$; Both the RAO and wave spectrum are only defined for a limited frequency range.

4.2. Measured Response Spectrum

The vessel motion response is measured in the time domain. An example of such a time series can be seen in figure 4.6. To be able to compare the measured response to the calculated response spectrum, a response spectrum is created from the the measured response time series. This is done by means of a Fourier Transform. The reliability of the spectrum that is obtained from one record, is very low. The error, which is the difference between the expected variance density $\frac{1}{2}a^2$ and the computed variance density $E\{\frac{1}{2}a^2\}$, is in the order of 100%, see figure 4.4. The large error exists because the variance density is estimated from only one amplitude per frequency.

In order to create a spectrum that is statistically more reliable, the signal is cut in to p segments of equal length, to create multiple segments of the same measurement as is shown in figure 4.6. As the number of segments p increases, the error decreases approximately by a factor \sqrt{p} [12].

$$error = \frac{\frac{1}{2}a^2 - E\{\frac{1}{2}a^2\}}{E\{\frac{1}{2}a^2\}} \approx \frac{100\%}{\sqrt{p}} \quad (4.3)$$

Based on the number of segments, the error reduces, so the reliability interval becomes smaller. Figure 4.5 shows the 90% confidence interval. This confidence interval is based on the assumption that the amplitude has a Rayleigh distribution (the wave height is assumed to have a Rayleigh distribution, and the motions are assumed linearly dependent on wave height). The amplitude squared thus has an exponential distribution.

However, as the number of segments increases, the frequency resolution Δf decreases, as can be seen in

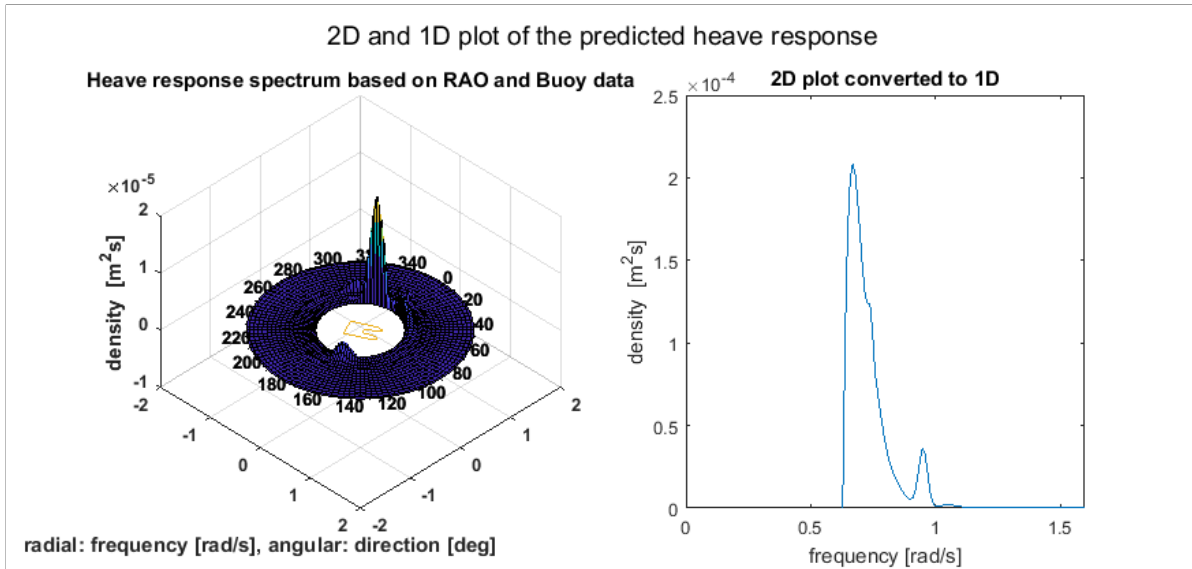


Figure 4.3: Example of heave response spectrum in 2D and transformed to 1D

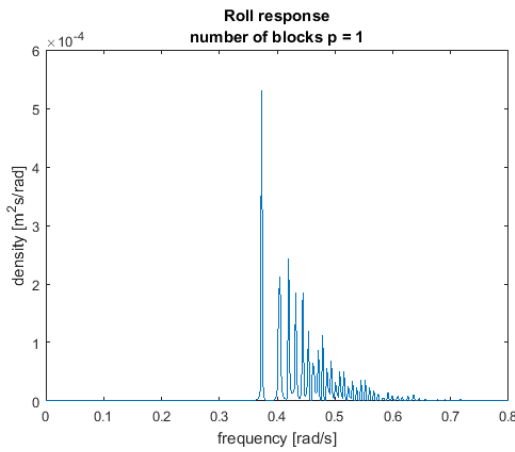


Figure 4.4: Roll response spectrum estimated from a single time series, meaning the variance density is calculated from one amplitude at each frequency. The error associated with estimating the variance density $\frac{1}{2}a^2$ by $E\{\frac{1}{2}a^2\}$ is in the order of 100%.

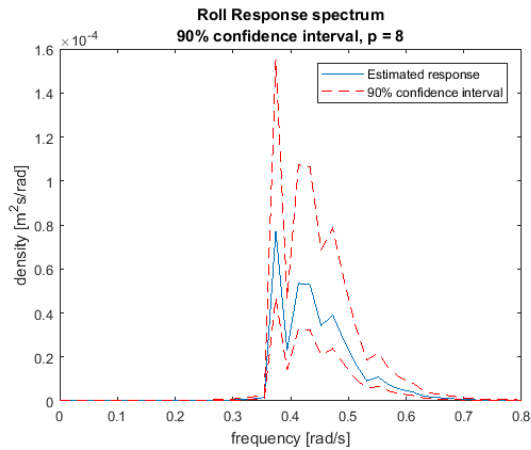


Figure 4.5: The estimated roll response spectrum, with the 90% confidence interval. The size of the confidence interval depends on the number of segments p

table 4.1. This means that a smaller error causes a lower frequency resolution, and there has to be a trade off between the error and the frequency resolution. A more detailed explanation of the Fourier Transform can be found in Appendix A

4.3. Comparing Spectra

From the 1D response spectrum, statistical parameters can be calculated. For the comparison of the predicted and measured spectra, two parameters are very important to compare: the significant double amplitude SDA and the peak period T_p . This is shown in figure 4.7. Moments can be calculated as follows:

$$m_{n\zeta} = \int_0^\infty \omega^n S_\zeta(\omega) d\omega \tag{4.4}$$

In which $m_{n\zeta}$ is the n -th order moment of the spectrum S_ζ , ω is the frequency and ζ is the degree of freedom. The zero-th order moment is the area under the spectrum, as shown in figure 4.7. With the zero-th order moment, the significant double amplitude of the response is calculated by:

$$SDA = 4\sqrt{m_0} \tag{4.5}$$

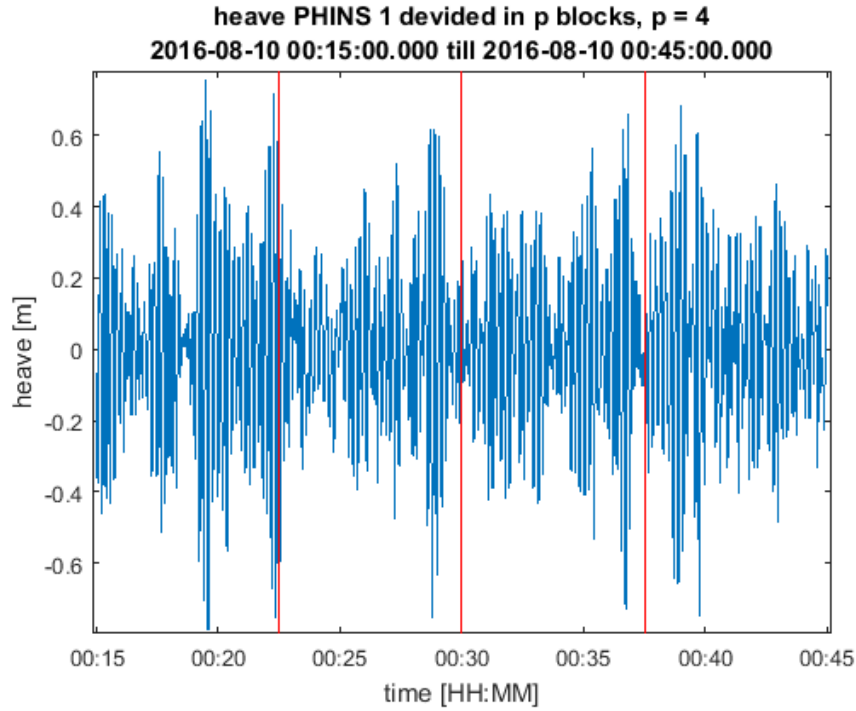


Figure 4.6: Half hour of measured heave motion at PHINS 1, divided in 4 segments of equal length

Table 4.1: Specifics of a half hour time series, and the specifics per block

Parameter	Half Hour time series		Per block	
	Symbol	Value	Symbol	Value
sampling time [s]	Δt	0.25	Δt	0.25
sampling frequency [Hz]	f_s	4	f_s	4
Nyquist frequency [Hz]	f_{Nyq}	$\frac{1}{2\Delta t}$	f_{Nyq}	$\frac{1}{2\Delta t}$
Number of time points [-]	N_{tot}	$4*60*30=7200$	N_{block}	N_{tot}/p
Duration [s]	D_{tot}	1800	D_{block}	D_{tot}/p
Frequency resolution	Δf	$1/D_{tot}$	Δf_{seg}	$p\Delta f$

The peak frequency is the frequency at which the spectrum has its highest value. The peak frequency ω_p has the units rad/s , another definition is the peak frequency f_p , with units Hz . Next to the peak frequency, the peak period T_p is often used. The relation is shown below:

$$\omega_p = 2\pi f_p = \frac{2\pi}{T_p} \quad (4.6)$$

Another commonly used parameter is the three hour maximum. The highest wave or motion that is expected to occur in three hours time. First, the number of waves are calculated. For this, the mean zero crossing period of the waves in a 3 hour window is used, which is calculated as:

$$T_z = 2\pi \sqrt{\frac{m_0}{m_2}} \quad (4.7)$$

Or alternatively, because the m_2 is sensitive to high frequency noise, another definition is sometimes used [12, p62]:

$$T_z = 2\pi \frac{m_0}{m_1} \quad (4.8)$$

In which T_z is the mean zero (up or down) crossing period of the waves, and m_0 and m_2 are the zero-th and second order moment respectively, calculated by formula 4.4. With the mean zero crossing period, the

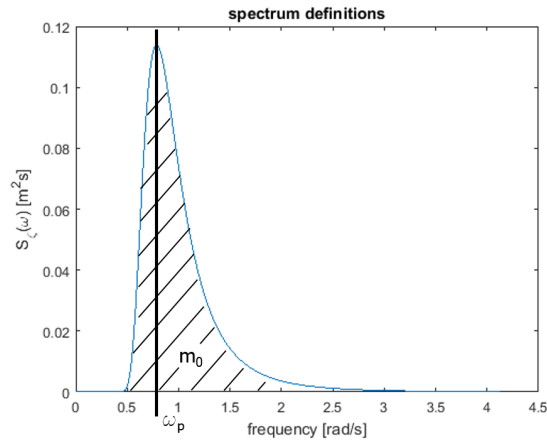


Figure 4.7: Parameters used to quantify a spectrum, m_0 is the zero-th order moment of the spectrum, ω_p is the peak frequency of the spectrum

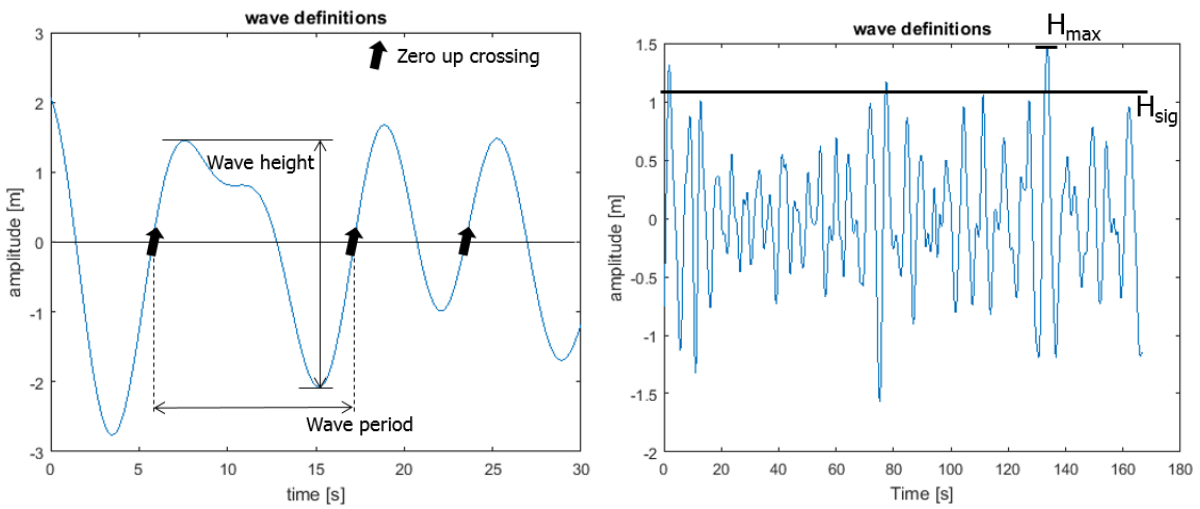


Figure 4.8: Wave definition by using zero-up crossing. a wave is defined between two consecutive zero-up crossings. Similarly, the mean of the highest one-third of the waves. The three hours maximum wave period is the period between two consecutive zero-up crossings. Figure 4.9: Wave definitions, the significant wave height H_{sig} is the mean of the highest one-third of the waves. The three hours maximum H_{max} is the most probable maximum waveheight in 3 hours time

number of waves N in three hours can be calculated:

$$N = \frac{3 * 3600}{T_z} \tag{4.9}$$

The three hour most probable maximum is then:

$$\zeta_{2mpm} = H_{max} = 2\sqrt{2m_0 \ln(N)} \tag{4.10}$$

In which ζ_{2mpm} is the most probable maximum double amplitude. The peak period T_p can be read from the spectrum: it is the period with the highest energy density.

5

Verification

In this chapter, the motion response calculation described in chapter 4 is verified. Two methods for calculating the response are compared, one in the frequency domain, and one in the time domain, which is then transformed to the frequency domain. These two methods should yield the same result. First, the methods are briefly explained, then the results are shown and next these results are discussed and conclusions are drawn.

5.1. Preliminary check

In order to verify the method of transforming the time series to a spectrum, a time series is created from a known JONSWAP spectrum. This is then transformed back to the frequency domain. To create a wave time series from a spectrum, the following formula is used [2, 5-45]:

$$\zeta(t) = \sum_{n=1}^N \zeta_{a_n} \cos(k_n x - \omega_n t + \varepsilon_n) \quad (5.1)$$

In which ζ is the wave elevation, ζ_{a_n} is the amplitude of the wave elevation, ω_n , k_n and ε_n are the frequency, wavenumber and phase shift for each frequency component n . The phase ε_n is chosen randomly from a uniform distribution between 0 and 2π . (The phases may not all be set to zero). Another realization of the time series, with different randomly chosen phases, will give the same spectrum S_ζ . The interval between two successive frequency components is $\Delta\omega$. The amplitude of the wave can be calculated from the wave spectrum, as follows:

$$\zeta_{a_n} = \sqrt{2S_\zeta(\omega)\Delta\omega} \quad (5.2)$$

The time series is translated back to the frequency domain as described in chapter 4. The original JONSWAP spectrum and the spectrum that was created from the time series, show a good comparison, as shown in figure 5.1.

5.2. Comparing time domain to frequency domain

Two methods for calculating the response are compared based on the same RAO and JONSWAP spectrum. In method one, a time simulation is done by the program AQWA Drift. In method two, a spectral approach in the frequency domain is used. The approach is schematically shown in figure 5.2. These two methods are then compared and should give the same results. The comparison is done for the motions in heave roll and pitch, for different peak periods of the JONSWAP spectra, and different incoming wave directions. For the time series, a duration of 5000 seconds is used and a time step of 0.5 seconds. The time series is divided into 20

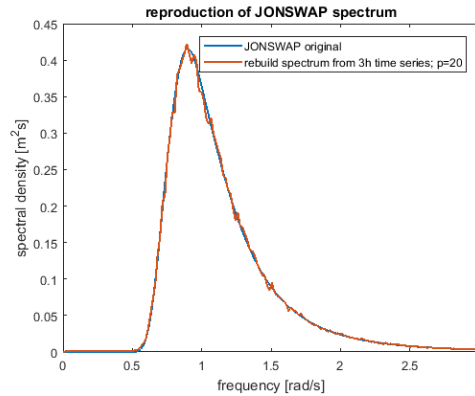


Figure 5.1: The original JONSWAP spectrum compared to the spectrum that is created from a time series

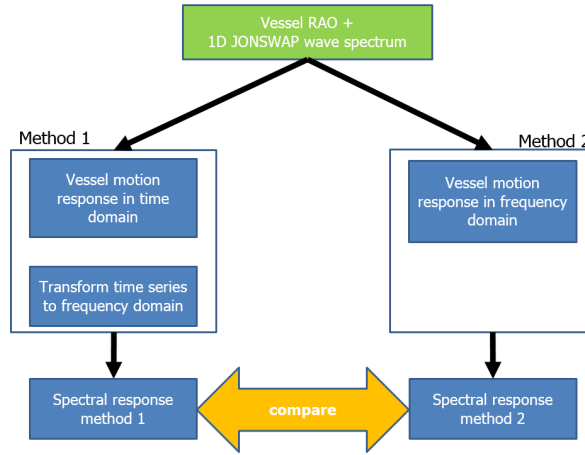


Figure 5.2: Explanation of method for comparing time domain simulation to spectral domain prediction

segments. This gives a spectral resolution of 0.25 rad/s. The response is calculated in time domain (method 1), based on an RAO and a given JONSWAP spectrum. For the RAO based position in time, the following formula is used [13, p. 28]:

$$x(t) = \text{Re} \left\{ \sum_{j=1}^{NSPL} \zeta_{a_j} x_j e^{i(-\omega_j t + k_j x_p + \varepsilon_j)} \right\} \quad (5.3)$$

in which:

- $NSPL$: number of waves in the spectrum
- ζ_{a_j} : the amplitude of the regular wave component
- x_j : the complex position at frequency ω_j i.e. the complex RAO
- ω_j : the j-th frequency
- k_j : the wavenumber at frequency ω_j
- x_p : the distance from the wave spectrum perpendicular to the wave direction
- ε_j : random phase at frequency ω_j

The amplitude of the regular component is calculated from the spectral ordinate that is given from the JONSWAP spectrum $S_\zeta(\omega)$ as follows [2, eq. 5-127]:

$$\zeta_{a_j} = \sqrt{2S_\zeta(\omega)\Delta\omega} \quad (5.4)$$

This gives the time signal for every time step. This can then be transformed to the frequency domain as previously explained in chapter 4. The calculation in the frequency domain is done as previously discussed in the same chapter. The comparison of the two methods is done for different wave directions and different peak periods of the JONSWAP spectrum, for the heave, roll and pitch. Figure 5.3 shows the result for the heave motion for a JONSWAP spectrum with $T_p = 12s$ and an incoming wave direction of 45 degrees. Figure 5.4 shows the same plot, but for a peak period of $T_p = 5s$. Results for the same periods and wave directions for roll and pitch are shown in figures 5.6 to 5.8. The comparison is very good for a wave spectrum with a peak period of 12 s. For a peak period of 5 s, the comparison is not very good. The frequency range that is chosen is based on the JONSWAP spectrum. The spectrum is divided in segments of equal energy, based on the zeroth order moment. This means that the frequency step is small for frequencies with high energy density, and large for frequencies with low energy density. Figure 5.9 shows the pitch RAO for a wave direction of 45 degrees, and the JONSWAP spectrum with a peak period 5 seconds. The same plot for a peak period of 12 seconds is shown in figure 5.10. It can be clearly seen that for a peak period of 12 seconds, the peaks of the RAO and the wave spectrum are almost at the same frequency. This cause a larger response, compared to the period of 5 seconds. From the comparison it can be seen that for larger peak periods, the time domain and frequency domain compare quite well. On the other hand, for higher peak periods, the comparison is worse. However, the amplitude of the response is also much smaller, The RAO is very small at the frequencies where the wave spectrum is significant. In practice, this will lead to small motions, thus being less important from a practical point of view. AQWA Drift selects the frequencies for calculation based on the JONSWAP spectrum. The zeroth order moment is calculated, and then the frequencies are divided such that each frequency element has an

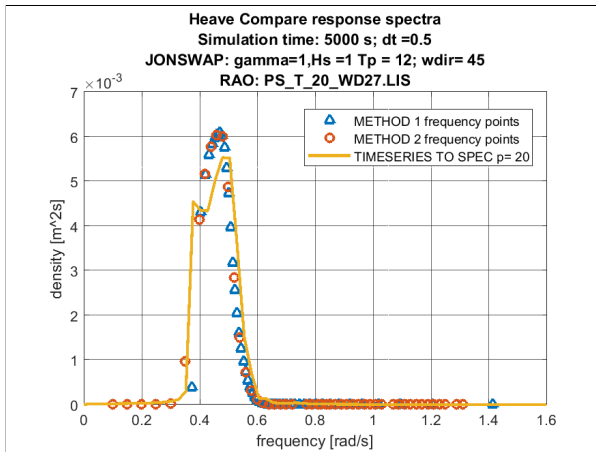


Figure 5.3: Comparison of heave response spectra, calculated in the frequency domain and in the time domain

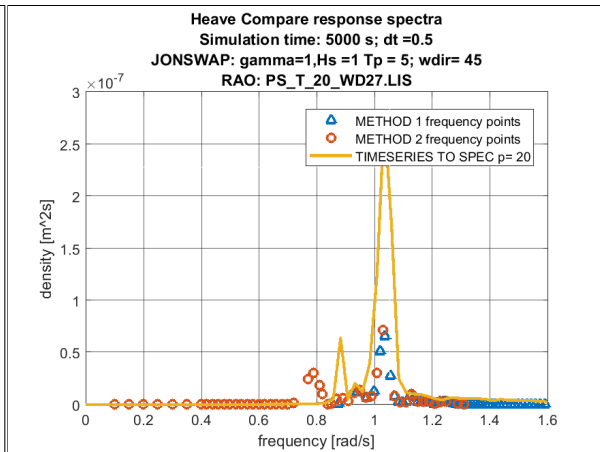


Figure 5.4: Comparison of heave response spectra, calculated in the frequency domain and in the time domain

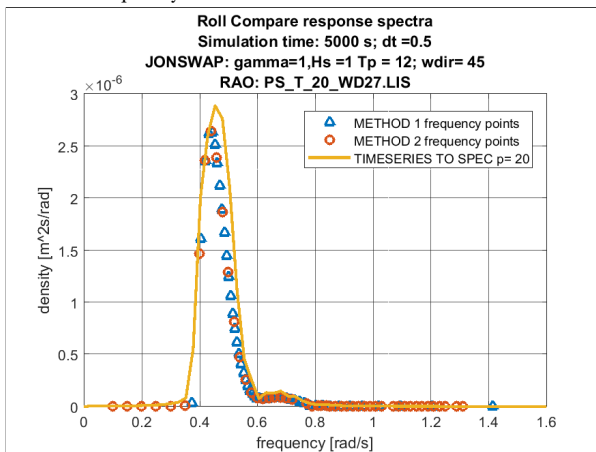


Figure 5.5: Comparison of roll response spectra, calculated in the frequency domain and in the time domain

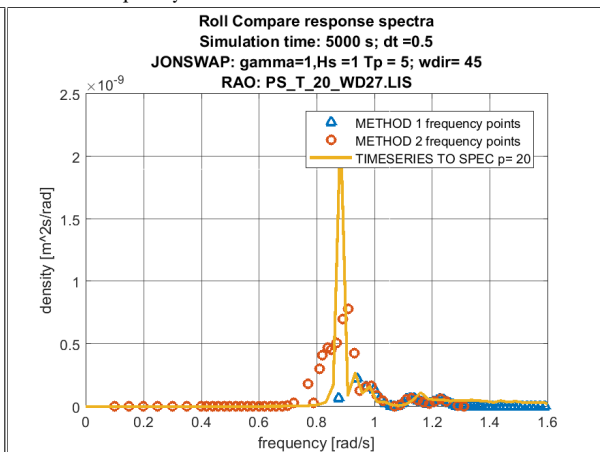


Figure 5.6: Comparison of roll response spectra, calculated in the frequency domain and in the time domain

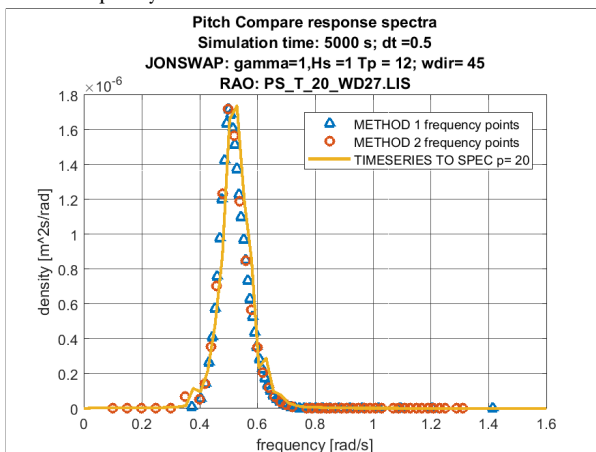


Figure 5.7: Comparison of pitch response spectra, calculated in the frequency domain and in the time domain

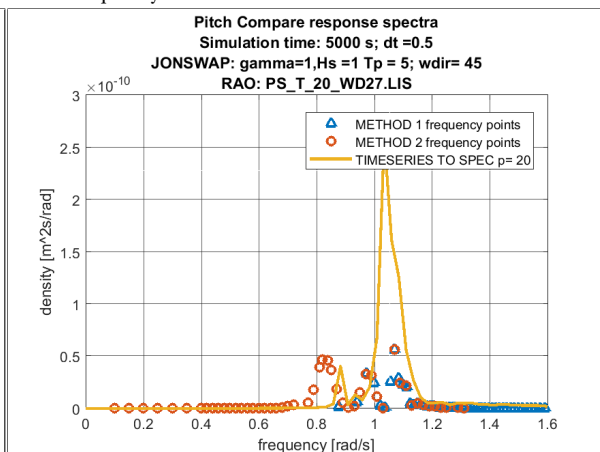


Figure 5.8: Comparison of pitch response spectra, calculated in the frequency domain and in the time domain

equal part of the m_0 . This means that for high density of the spectrum, the frequencies are close to each other, and for low density, the frequency step becomes larger. From this we can conclude that the peak period of the wave spectrum is important for a good prediction. In most cases, the peak in the RAO is at a lower frequency than the peak in the wave spectrum. The closer the peak of the RAO and the wave spectrum are, the better the prediction gets. So a higher peak period T_p of the wave spectrum, means a better prediction in general.

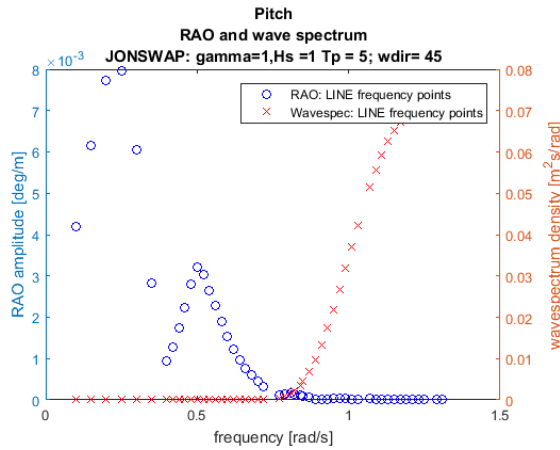


Figure 5.9: Pitch RAO and JONSWAP wave spectrum frequency points used in the calculation for $T_p = 5s$, wave direction is 45 degrees

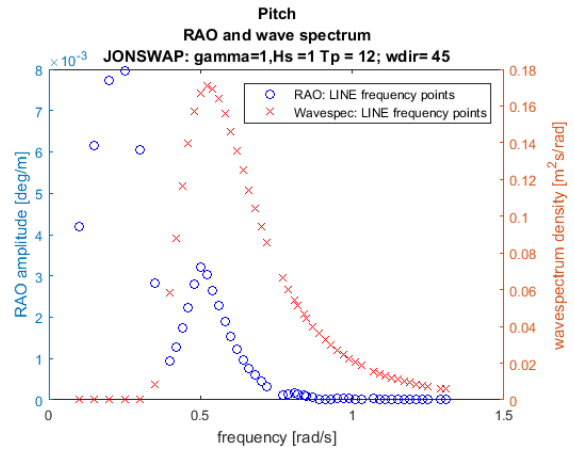


Figure 5.10: Pitch RAO and JONSWAP wave spectrum frequency points used in the calculation for $T_p = 12s$, wave direction is 45 degrees

5.3. Sensitivity Analysis

Influence of number of segments

The number of segments that is used in the calculation, is varied. A larger number of segments gives a spectrum with higher reliability. The influence is investigated by simulating the response calculation for various number of segments, and looking how it influences the SDA and the peak period. Figure 5.11 shows the result for the three hours maximum. the change from one block to 100 segments is 3%. So the number of segments does not significantly change the calculation of the 3 hours maximum. For the peak period, there is a significant change dependent on the number of segments used in the FFT. The result is shown in figure 5.12. The peak period changes quite drastically. This can be explained as follows: as the number of segments increases, the energy gets averaged over a larger frequency interval. One high narrow peak (for example low frequency peak in figure 5.16) can get averaged out, causing the peak period to change.

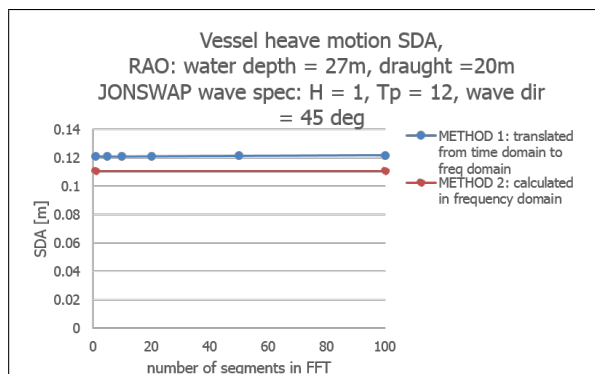


Figure 5.11: Influence of the number of segments used in the Fast Fourier Transform (FFT) on the SDA, the graph shows the influence is small.

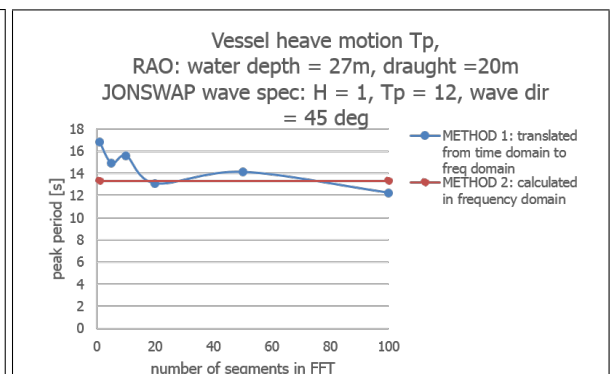


Figure 5.12: Influence of the number of segments used in the FFT on the peak period. The peak period varies strongly dependent on the number of segments used.

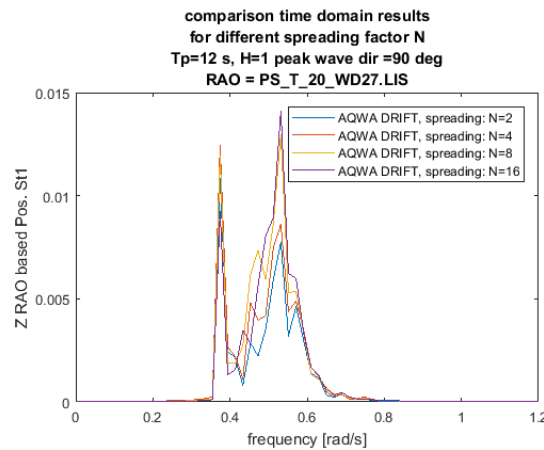


Figure 5.13: Comparison of response spectra translated from time domain to frequency domain, for different wave spreading in the JONSWAP spectrum

Influence of wave spreading

The JONSWAP spectrum can have a different spreading factor. The influence of a different spreading on the response is investigated. The total energy in the spectrum is constant. However, as the RAO changes over the direction, it can be expected that a different spreading factor also gives a different response. This can indeed be seen in the comparison of figures 5.14 and 5.15. It can also be seen that the response does hardly change from a spreading factor of 8 to 16. This can be explained by the fact that as the spreading factor goes up, the spectrum is looking more and more like a 1D wave spectrum, and the RAO is taken for a smaller directional spread.

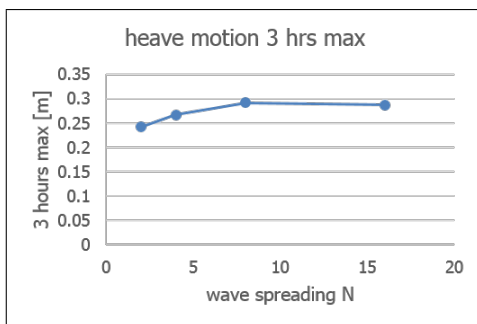


Figure 5.14: Influence of the spreading factor in the JONSWAP spectrum on the 3 hours maximum

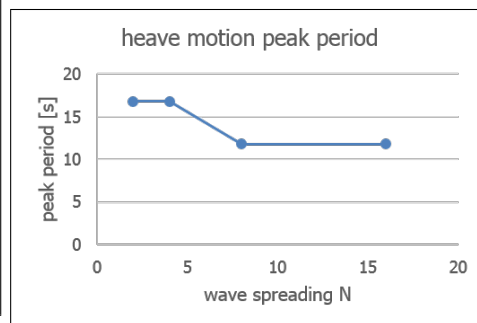


Figure 5.15: Influence of the spreading factor in the JONSWAP spectrum on the peak period

Influence frequency smoothing

A slightly different method for translating the time series to a spectrum involves frequency smoothing. The method described in chapter 4 is compared to the method which uses frequency smoothing. This method is also based on dividing the time series in segments, to which a Parzen window is applied. The time series is multiplied by the Parzen window, causing a smoother result if the signal is then transformed to the frequency domain [14]. The results of comparing the methods is shown in figures 5.16 to 5.19. The method with and without frequency smoothing give similar results for the m_0 . As the number of segments increases, the T_z is varying less for the method which uses frequency smoothing. The method for calculating T_z is as described in formula 4.8, to be less sensitive to high frequency noise. Another conclusion that can be drawn is that as the spectrum becomes more smooth, less details can be distinguished.

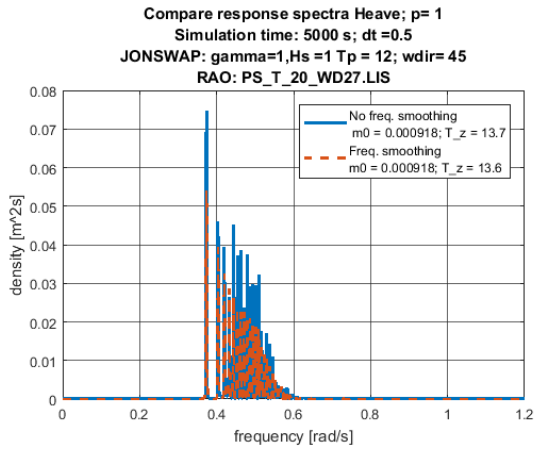


Figure 5.16: Comparison of spectra created from time series, were the time series is split into one block (p=1)

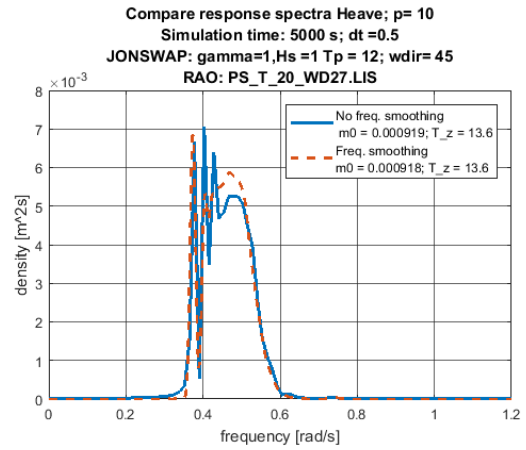


Figure 5.17: Comparison of spectra created from time series, were the time series is split into ten segments (p=10)

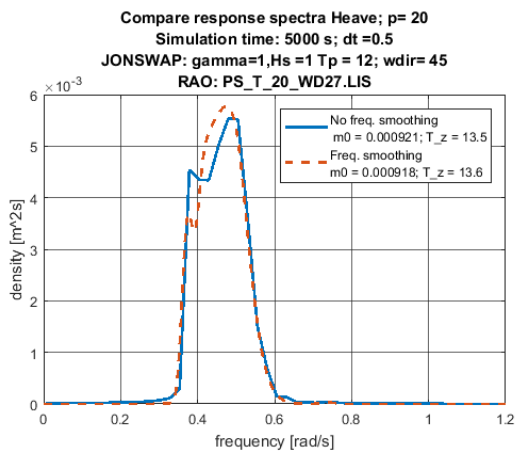


Figure 5.18: Comparison of spectra created from time series, were the time series is split into twenty segments (p=20)

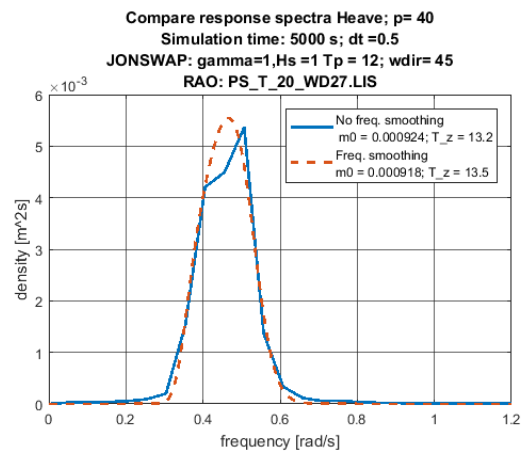


Figure 5.19: Comparison of spectra created from time series, were the time series is split into fourty block (p=40)

5.4. Conclusions

Based on the verification study, the following conclusions can be drawn with respect to the calculation method:

- The method of translating a wave time series to a spectrum in the frequency domain is validated.
- Using the same method for calculating the response spectrum of a vessel from a time series is validated for limited situations.
- The method does work if the peak frequency of the RAO and the wave spectrum are close to each other (figure 5.10) If this is not the case (figure 5.9), the method could not be validated, due to the used software.
- For calculating the SDA, the method is not sensitive to the amount of segments used in the translation from time domain to frequency domain. 5.11
- For calculating the peak period T_p , the method is very sensitive to the amount of segments used, choosing different amount of segments can lead to a different peak period 5.12.

6

Analysis of input data

The input data for the comparison between measured and predicted vessel motions, needs to be evaluated carefully. The accuracy of the input data limits the accuracy that can be obtained for the output. The different input parameters for the comparison are analysed. These are, for the prediction, the 2D wave spectrum, the 2D RAO and the vessel heading and for the measurement the measured time series, as shown in figure 6.1. The heading is measured by the same sensors that measure the time series vessel motions, and thus the heading will be discussed together with the measured time series.

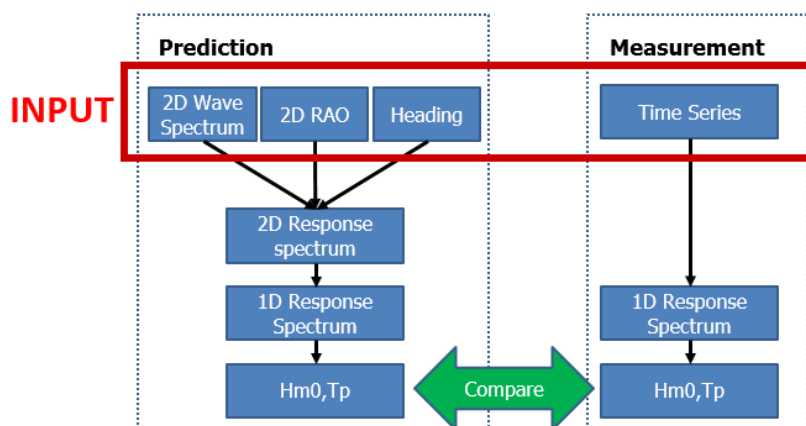


Figure 6.1: The approach for comparing predicted and measured vessel motions. The input section will be discussed in this chapter.

6.1. Available data

Because the *Pioneering Spirit* is relatively new vessel, the amount of vessel motion measurements is limited. Data of a few offshore operations is available. So far there have been 4 operations of which data is available. At one of these, a wave buoy was present to measure the two dimensional wave field. The available data is summarized in table 6.1. During these measurements, the vessel can be performing tasks like ballasting, connecting to the platform, rotating for offshore testing and so on. These vessel operations influence the vessel's response. Data about these tasks is available, and this can be used to see whether a predicted motion is expected to be influenced by the vessel operations. The Offshore Acceptancy Test One (OAT1) will be the starting point of the analysis because the available data is for a relatively long time period, and the presence of the buoy gives the best possible description of the wave spectrum, more accurate than the wave spectrum from a forecast. During OAT1, the *Pioneering Spirit* is located on the North Sea between the Netherlands and the UK, as shown in figure 6.2.

Table 6.1: Available vessel motion data, at OAT1, a buoy is present giving a very good wave spectrum

date	name	location	water depth	type of data
09-08-2016 to 16-08-2016	OAT1	North Sea	27 m	forecast + vessel motions + buoy



Figure 6.2: Location of measurements on the North Sea during Offshore Acceptancy Test 1 (OAT1)

6.2. 2D wave spectrum

The two-dimensional wave spectrum can be obtained by means of a buoy or by means of a forecast. For OAT1, a buoy is present. The buoy is deployed at a location close to the vessel, at a distance of approximately 1 km. The buoy cannot be too close because the waves created by the vessel's own motions should not be measured, and the vessel should not cause shielding of the waves measured by the buoy. This means there is some distance between the buoy and the vessel, and the wave field will differ a bit between the location of the buoy and the vessel location. However, if the location of the buoy is selected properly, the buoy will give a good representation of the wave field at the location of the vessel. The forecasted two dimensional wave spectrum is based on computer models. Contrary to a buoy, it is not a real measurement. Its advantage with respect to the buoy is that spectra for the future are available. Using these spectra, it is decided whether or not an offshore operation can take place. The forecast predicts the weather for a few days ahead. If the weather is stable, the forecasted wave spectrum for a given time does not vary much. On the other hand, in unstable weather, the forecasted spectrum for a given time might change, which means the forecasted spectrum is less reliable. To see whether a predicted motion agrees with a measured motion, less uncertainty is introduced if the predicted motion agrees with the motions calculated based on the spectra from a buoy. Therefore, the buoy is selected as a first way to check how the comparison agrees with the measured motions.

Wave Buoy Specifics

The buoy used at this location is a TRIAXYS wave buoy, the specifications of this buoy are shown in table 6.2. On board this buoy the measured time series of the wave elevations are processed, and the output that is available from the buoy is a wave spectrum for every half hour. This means no raw time series from the buoy are available. This is the reason the measured vessel motions also need to be transformed to a spectrum, which is described in chapter 4. The wave spectrum is given as a function of direction in degrees and the frequency in radians per second, see top plot of figure 6.3. The frequency axis of the wave buoy spectrum has a constant step, this means the period step size increases as the period increases, as is shown in the bottom plot of figure 6.3. For example, for a period of 5 seconds, the step is around 0.3 seconds, while for a period of 10 seconds, the the step is around 1 second. Therefore, the spectrum is less detailed for longer periods. This is very important, because the vessel response has more energy for the relative high periods in the wave spectrum. The wave spectrum gives the spectral density for a range of frequencies (the resolvable frequencies), for a range of directions. The frequency range is split in sections. Only the sections that hold at

Table 6.2: Specifics of the TRIAXIS Next Wave II Directional Wave Buoy

Parameter	Range	Resolution	Accuracy
Wave Height/heave	± 20 m	0.01 m	better than 1%
wave period	1.5-33 s	0.1 s	better than 1%
Direction	0-360 deg	1 deg	3 deg
2D spectrum output			
frequency range	variable	rad/s	
frequency step	0.063	rad/s	
directional step	3	degrees	

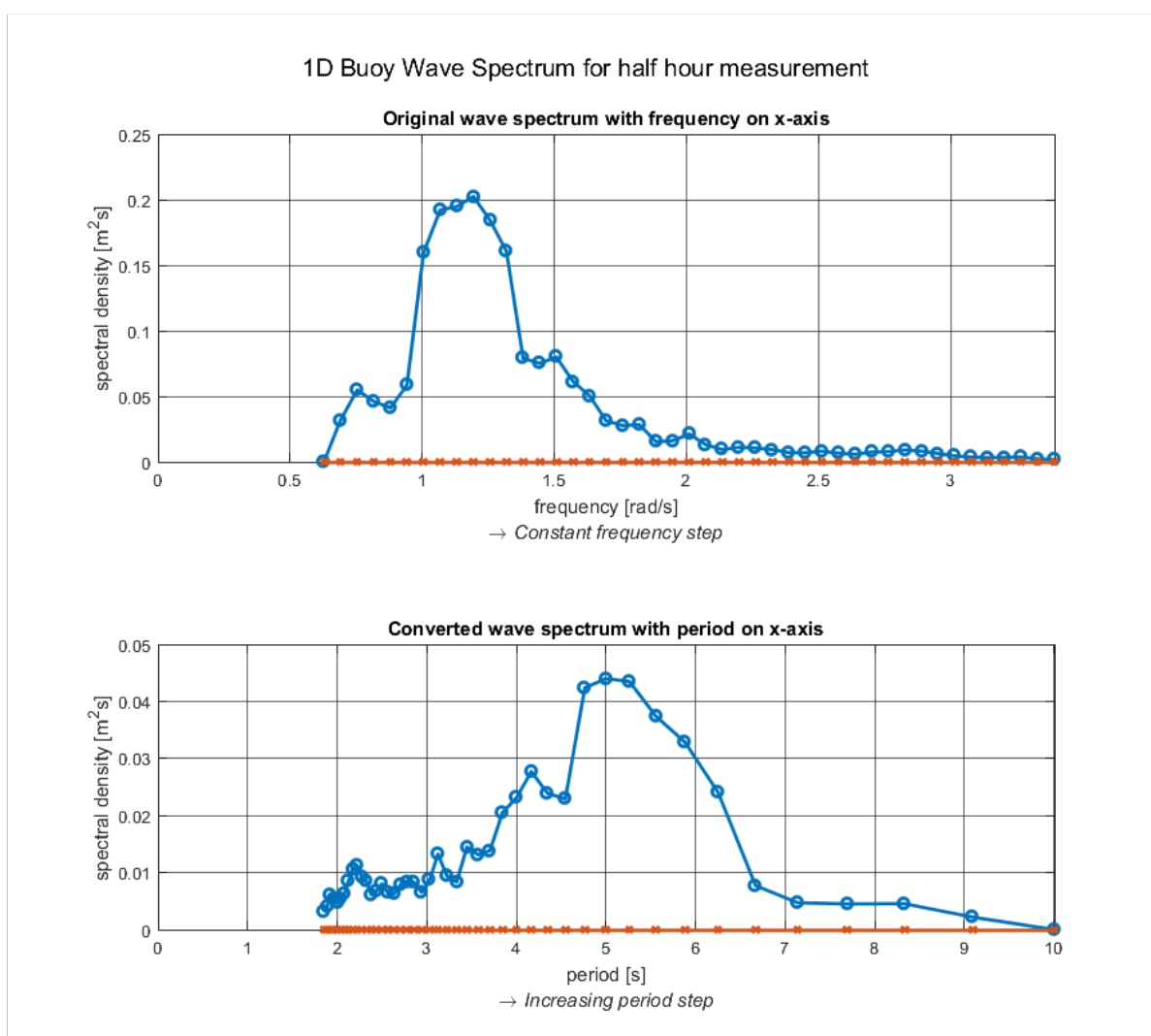


Figure 6.3: Example of a 1D buoy wave spectrum during OAT1. The top plot shows the spectrum, with the frequency in rad/s on the x-axis and a constant step in the frequency, as given from the buoy. Converting this spectrum to a spectrum with the period on the x-axis, as in the bottom plot, shows an increasing period step as the period increases. This means the spectrum is more detailed for low periods and less detailed for higher periods.

least a minimum threshold of energy, are taken into account for the spectrum calculation. This also means that frequencies that hold less than this threshold of the total energy, are not taken into account. This is known to have caused problems during OAT2, where a very small swell peak was neglected by the buoy, leading to a wrong prediction of the motions. Once the total energy of the wind sea waves decreased, the swell peak was noticed by the buoy and the predictions improved significantly.

Double-peaked spectra

Typically, a wave spectrum is described by the significant wave height H_{m0} and the wave period T_p and the peak wave direction. However, if more peaks occur in the spectrum, the spectrum should be described by the H_{m0} and T_p per peak. An example of the 2D spectrum from the buoy is shown in figure 6.5. The figure shows the primary and secondary peak of the wave spectrum. The direction of the primary peak (the peak largest peak in the spectrum) is called the peak wave direction. Dependent on the amplitude of the RAO for the primary and secondary peak, the contribution to the response can be larger for the direction of the secondary peak. If these two peaks have almost the same magnitude, the peak direction can change suddenly from one direction to the other. This is observed in the plot for the peak incoming wave direction on 11-08, see figure 6.5, where the primary peak becomes the secondary peak and vice versa. Looking only at the peak direction of the waves may lead to wrong interpretation of the result if the secondary peak has significant energy, especially if this secondary peak occurs for a direction with a higher RAO.

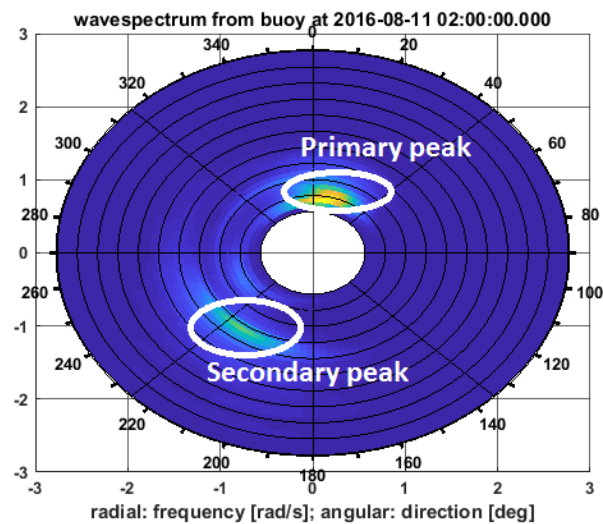


Figure 6.4: Example of a directional wave spectrum obtained from the TRIAXIS Next Wave II Directional Wave Buoy, showing the primary and secondary peak coming from different directions.

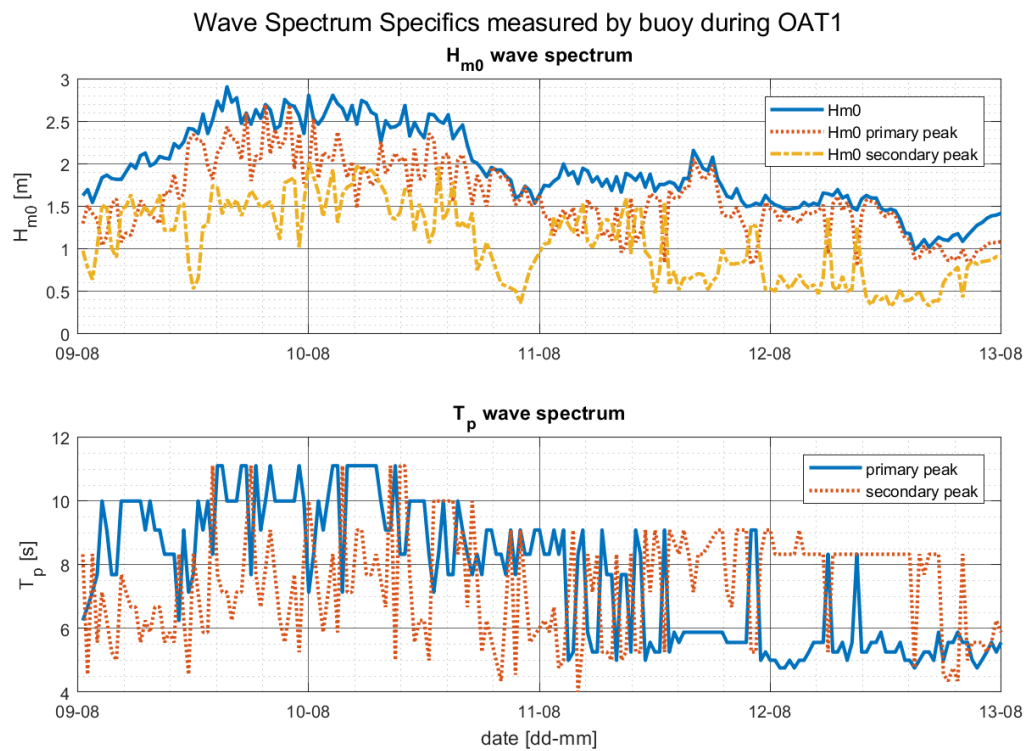


Figure 6.5: Wave spectrum specifics measured from the TRIAXIS Next Wave II Directional Wave Buoy. The top plot shows the significant amplitude of the 1D wave spectrum, and the significant amplitude of the primary and secondary peak. The bottom plot shows the peak period for the primary and secondary peak.

6.3. 2D RAO

The vessel's RAOs are calculated using potential theory as was described in chapter 3. The minimum frequency that can be calculated is found from the formula:

$$\omega_{min} = 0.001 * \max(1, \sqrt{\frac{g}{h}}) \quad (6.1)$$

In which g is the gravitational acceleration and h is the water depth. The maximum frequency for which the RAO can be calculated, depends on the element size of the vessel. The vessel is modelled with a certain amount of elements, see figure 6.6. The size of these elements determines the minimum wave length for which the RAO can be calculated:

$$\text{Element Size} < \frac{1}{7} L_{min} \quad (6.2)$$

In which L_{min} is the minimum wave length. The maximum corresponding wave frequency can be calculated from the wave length. However, the minimum and maximum frequencies in the RAO do not limit the response, because the minimum allowable frequency is well below the minimum frequency of the wave spectrum, and the maximum frequency is above the maximum frequency of the wave spectrum. The RAO depends on the draught of the vessel. The draught is measured on four locations on the vessel, on the fore and aft, both on port side and starboard. The results are shown in figure 6.7. Due to a small trim and roll angle, the measurements do not measure the same water depth. Because the water depth is slightly different for starboard and portside, mirroring the RAO gives a small error. At the location of the measurements, the water depth is 27 m. With a draught up to 21 m, a water depth of 27 m and the large dimensions of the *Pioneering Spirit*, the question arises whether this can be adequately solved with potential theory and the description of point sources. However, looking at the RAO for different water depths, show no sudden unexpected changes in the RAOs for shallow water depth compared to deeper water which could indicate a mathematical problem in the software, and therefore the theory seems to work even for the relatively small water depth.

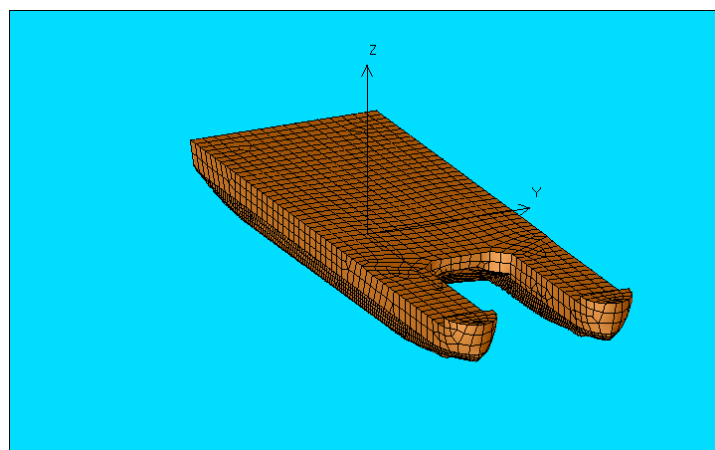


Figure 6.6: Mesh of the *Pioneering Spirit*, the element size determines the minimum wave length for which the RAO can be calculated.

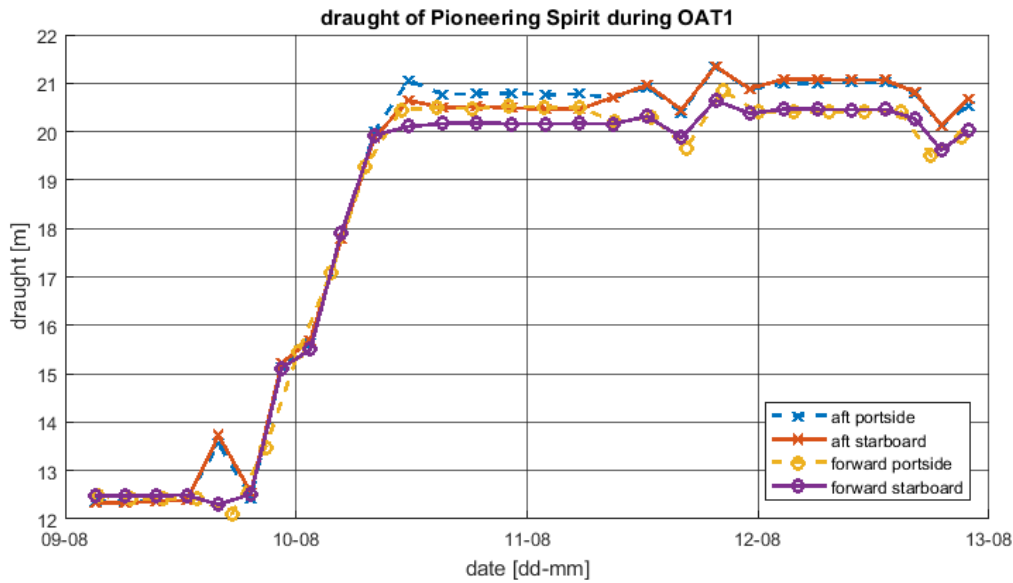


Figure 6.7: Draught of the *Pioneering Spirit* measured on fore and aft both on starboard and port side.

RAO for changing water depth

As the water depth changes, the RAO changes as well. Appendix ?? shows more details of the RAOs for different water depths and wave directions. As well as the influence of the water depth on the RAO, added mass, potential damping and wave forces for the heave, roll and pitch.

Heave RAO

Figure 6.8 shows how the RAO of the *Pioneering Spirit* changes with the water depth for heave with wave directions from 90 degrees. The deep water RAO is also shown (water depth = 1000 m). The figure shows that for a small change of 1 m in water depth, the RAO can change significantly, both in amplitude and shape. Comparing the shallow water to deep water, the peak occurs at lower frequencies for shallow water. The first peak (at lower frequencies) becomes larger as the water is more shallow. The second peak however, is smaller for shallow water depth. This means that the vessel will react less to high frequency waves in shallow water, compared to deep water.

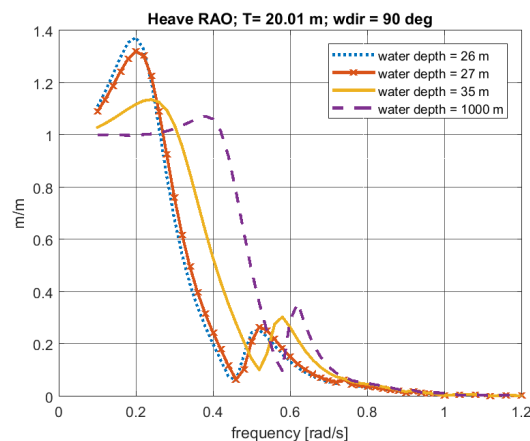


Figure 6.8: Heave RAO for different water depths, wave direction is 90 deg.

Roll RAO

The roll RAO is largest for a wave direction of 90 degrees. This RAO is shown in figure 6.9. For the roll, similar as for the heave, the RAO shifts towards higher frequencies for an increasing water depth. Looking at the roll

for 90 degrees, the peak decreases as the water depth increases from 26 to 35 m, but the peak increases as the water depth increases further to deep water of 1000 m.

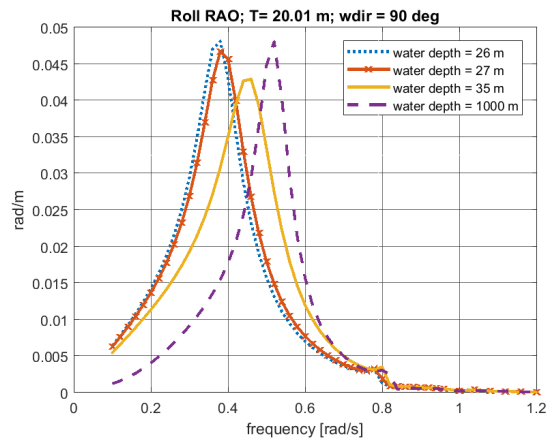


Figure 6.9: Roll RAO for different water depths, wave direction is 90 deg.

Pitch RAO

The RAO for the pitch is shown for a direction of 45 degrees incoming waves in figure 6.10. Two peaks are present, one at low frequencies, which is decreasing in amplitude and shifting to higher frequencies as the water depth increases. The second peak, at higher frequencies, shows the same trend. This peak shifts strongly for a changing water depth. An increasing water depth causes the second peak to shift towards higher frequencies.

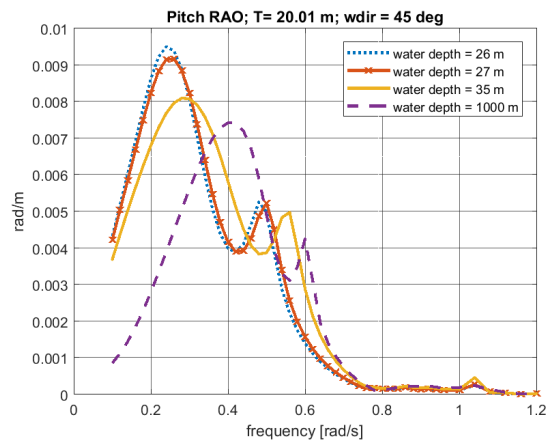


Figure 6.10: Pitch RAO for different water depths, wave direction is 45 deg.

Added Mass and Potential damping

The RAO depends on the added mass, potential damping, and the incoming wave forces. In general, the trend is that for deeper water, the RAOs shift to higher frequencies. In chapter 3 it was found that this shift can be caused by a change in added mass and potential damping. Figure 6.11 shows the added mass a_{33} , for changing water depth for the heave. The added mass increases for decreasing water depth, as was already expected from literature[4]. The increase in added mass is the strongest for the heave motion, the added mass a_{33} is almost 5 times as high for a water depth of 27 m, compared to the deep water case of 1000 m. At a certain frequency, between 0.6 and 0.7 rad/s, there is a sudden change in the added mass, especially visible for the a_{33} and a_{44} , see ???. This has to do with the shape of the *Pioneering Spirit*. For a certain frequency, a standing wave occurs between the two bows of the vessel, causing the sudden change in added mass. This cancels with the potential damping, which has a peak at the same frequency. The added mass and damping

are the real and imaginary part of the same function, see formulas 3.16 and 3.17. The peaks in added mass and potential damping are thus not visible in the RAO. The potential damping is shown for the heave in figure 6.12. The potential damping also is changing strongly with a change in water depth, and it shows peaks at the same frequencies as the added mass, due to the standing wave occurring between the bows of the vessel.

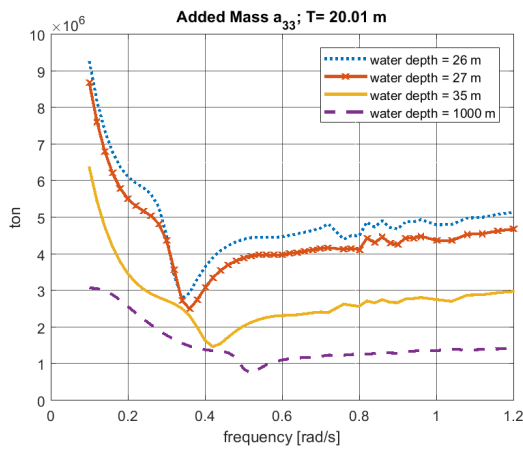


Figure 6.11: Added mass a_{33} for different water depths

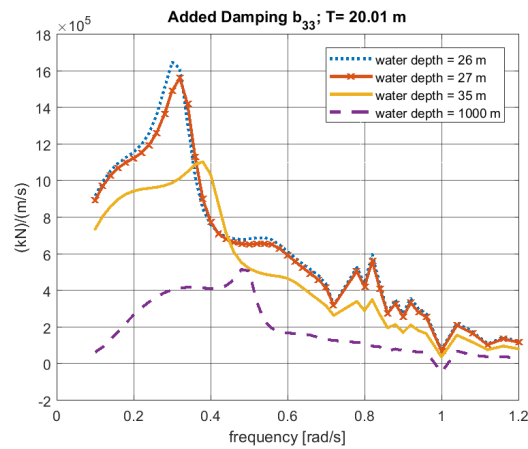


Figure 6.12: Added damping b_{33} for different water depths

Wave Forces

The wave forces, consisting of the Froude-Krilov and the diffraction forces, are shown in figure 6.13 for the heave for a incoming wave at 90 degrees. The wave force is changing for different water depths, especially for low frequencies. The difference between deep water and shallow water is significant for low frequencies. the difference for 1 m of water depth at higher frequencies (0.7 rad/s) is relatively small.

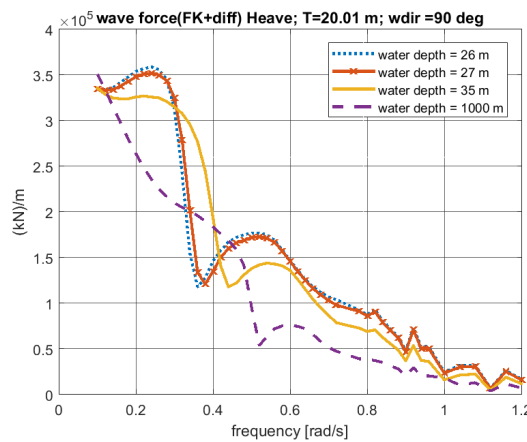


Figure 6.13: Total wave force (Froude-Krilov and diffraction) in the heave direction for a wave direction of 0 degrees

Heave RAO at sensor location

To predict the heave motions at the location of the sensors, the RAO is translated from the Central Reference Point (CRP) to the sensor location using rigid body motions. As the distance from the CRP increases in x-direction, the contribution of the pitch to the heave motion increases. Therefore, the contribution of the pitch motion will be larger for heave at the location of Motion Reference Unit (MRU) PHINS1 than on MRU PHINS4. The roll contribution to the heave motion increases as the distance in y-direction increases. MRU PHINS1 and PHINS4 have the same distance to the CRP, so the contribution of the roll will be the same for heave at PHINS1 and heave at PHINS4. The amplification due to the distance from CRP are shown in table 6.3.

	heave at PHINS1	Heave at PHINS4
1 m heave at CRP	1 m	1 m
1 deg roll	$31 * \pi/180 = 0.54$ m	$31 * \pi/180 = 0.54$ m
1 deg pitch	$164 * \pi/180 = 2.86$ m	$69 * \pi/180 = 1.20$ m

Table 6.3: amplification factor for heave roll and pitch for the locations PHINS1 and PHINS4 due to distance from CRP

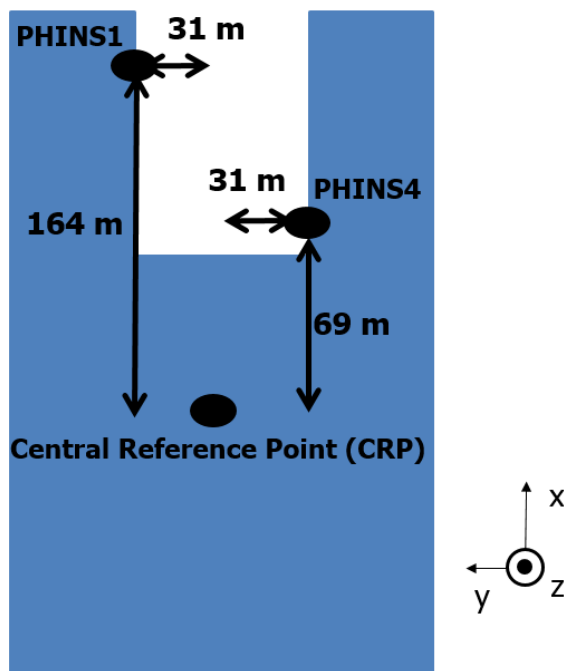


Figure 6.14: Location of sensors onboard *Pioneering Spirit*. The heave RAO at the sensor locations is constructed from the heave RAO at the Central Reference Point (CRP), the roll and the pitch. A larger distance from the CRP in x-direction causes a larger contribution of the pitch RAO, and a larger distance from the CRP in y-direction causes a larger contribution to roll RAO to the heave RAO at the location of the sensor.

6.4. Time Series Measured

The vessel motions are measured on board of *Pioneering Spirit* on several locations. Several sensors have been checked for suitability of this study. It has been found that not all sensors had data available for the time period of interest, or the data is distorted. Based on the availability of data, two different sensors have been selected: PHINS1 and PHINS4, as can be seen in figure 6.14. These sensors measure (among others) the heave, roll, pitch and heading. The accuracy of these sensors is summarized in table 6.4. To compare the predictions based on the buoy data and the vessel measured time series, the same time interval needs to be selected. The buoy data has a wave spectrum every half hour, the time series is selected a quarter of an hour before and after the buoy time stamp, as shown in figure 6.15.



Figure 6.15: Selection of the time interval. The buoy has a time stamp every half hour, the time series is selected a quarter of an hour before and after the buoy time stamp

Table 6.4: Sensor accuracy for PHINS1 and PHINS4, measuring the heave, roll pitch and heading. The accuracy mentioned here accounts for both accuracy and precision.

Parameter	Accuracy
Heave	2.5 cm or 2.5% RMS (whichever is larger)
Roll	0.01 deg RMS
Pitch	0.01 deg RMS
Heading	0.01 deg 1/cosine latitude RMS

The accuracy is described in RMS value. The RMS error is defined as:

$$RMSError = \sqrt{\frac{\sum_{i=1}^n (\hat{y}_i - y_i)^2}{n}} \quad (6.3)$$

in which RMSError is the spreading of the measured value around the real value. \hat{y}_i is the measured value, and y_i is the real value, and n is the number of data points. It can be expected that 95% of the real values are within 2 times the RMS from the measured value [15].

pre-processing of the time series

The sampling of the time signal is based on accelerations. As soon as a change in acceleration is noticed, a new data point is created, so the sampling is done at a varying time interval. In order to do a proper Fourier transform, the signal has to be sampled at a constant time step. Therefore, the signal will be re-sampled. The re-sampled signal should have at most as much data points as the original signal [16]. It was found that for the data from the PHINS sensors, the average time step varies between 0.21 and 0.24 s. To stay within this limit, the signal is re-sampled at $\Delta t = 0.25$ s, see figure 6.16. The figure shows the comparison between the raw and interpolated time series of the roll motion for sensor PHINS1. similar comparisons are made for the heave and the pitch motions. It can be seen that the peak of the raw signal slightly deviates from the interpolated one, but the difference is very small. In general, this difference remains within 2% of the maximum value. The time signal should be small enough to capture effects that are of interest, and prevent aliasing. With the selected time step of 0.25 seconds, the Nyquist frequency is 2 Hz, or 12.57 rad/s. the vessel motions are practically zero well below this high frequency. Aliasing is not expected to be a problem due to the high Nyquist frequency. During the measurement, a temporary failure of the sensor can occur. For this time interval, no sensor data is available. This causes data gaps, which is shown for the heave motion in figure 6.17. If no data is available, the sensor does not show any data points. Similar plots can be shown for the other degrees of freedom. For the heading, the occurrence of a data gap is slightly different. If there is no measured signal, the heading then rapidly changes between zero and 360 degrees, which can be seen in figure 6.18. These intervals are removed from the data.

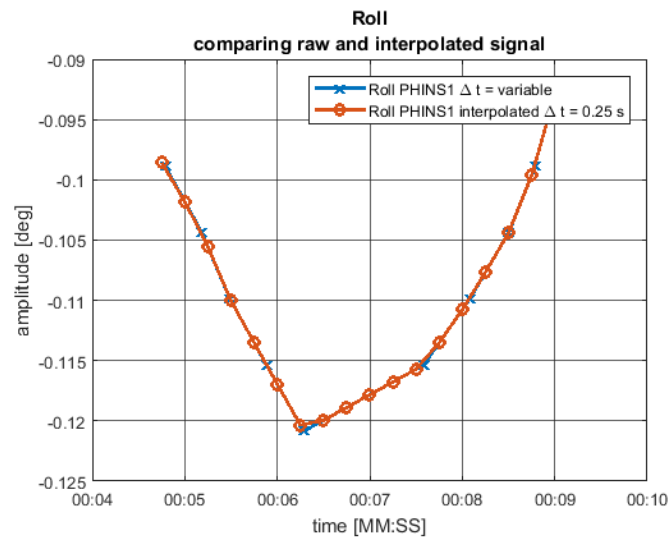


Figure 6.16: Roll measured at PHINS 1 and interpolated with $\Delta t = 0.25$ seconds. The graph shows a very small deviation between the peak of the raw and the interpolated signal

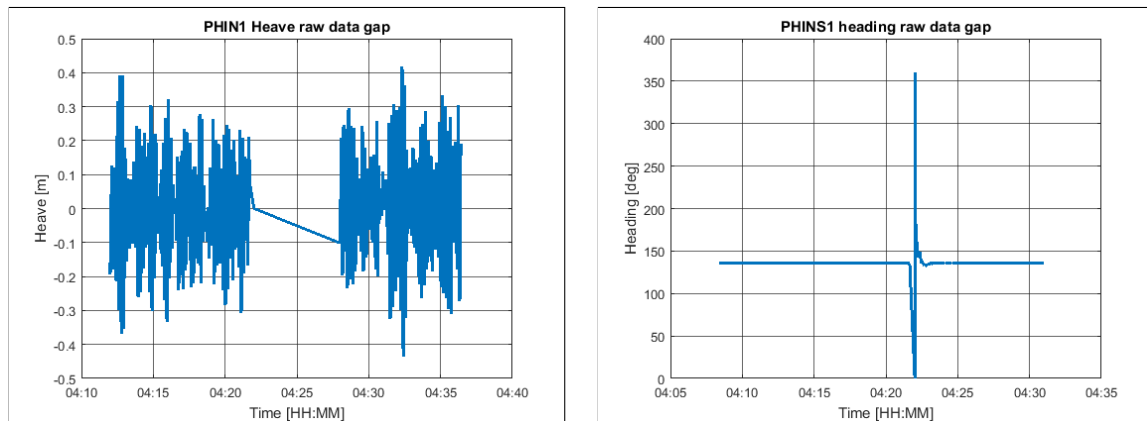


Figure 6.17: Raw heave motion measurement at PHINS 1, showing a data gap of several minutes Figure 6.18: Raw heading measurement at PHINS1. The signal jumps to 0 and 360 degrees if no data is available

The roll and the pitch do not (always) vary around a zero mean. The vessel can be heeling and trimming. This causes an offset in the roll and pitch respectively. Because the data will be translated from the sensor locations to another point on the vessel, the mean will be removed from the signals. This is shown in figure 6.19. First, a moving average is calculated, based on a certain number of data points. The amount of data points that is used, is dependent on the time interval of the time signal. If too many data points are used, short variations are not recognised as moving average. If not enough data points are used, longer variations (caused by second order movement for example) will be disregarded. The time signal here is interpolated for a time step of 0.25 seconds. For the calculation of the moving average, 4000 data points are used, which means a time trace of 1000 seconds. This means that variations with a period of more than 1000 seconds are not identified, this period is well above the vessel's eigenperiod.

6.5. Validation rigid body motions

The *Pioneering Spirit* is known to have bow deformations in some situations. This would mean that Rigid Body Motions are not valid in this case. In the prediction of the vessel motions, rigid body motions are assumed and need to be validated first. These assumptions can be validated by using the two sensors PHINS 1 and PHINS 4. To verify the rigid body assumption, first the roll and pitch are compared. These should yield the same results if the vessel moves as a rigid body. First, the moving average is removed from the time se-

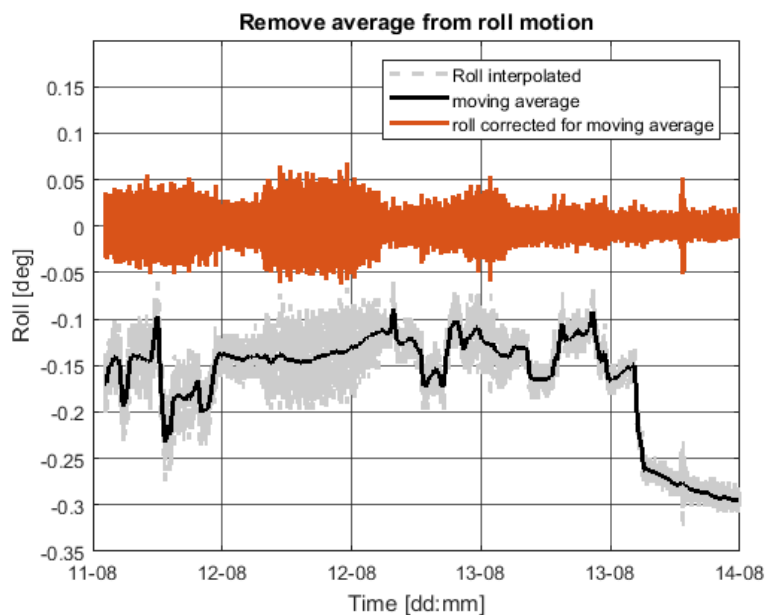


Figure 6.19: Removing average of roll motion of sensor PHINS1: The moving average is subtracted from the measurement signal, leaving a zero mean roll motion

ries, after which the roll and pitch for the two sensors are compared. The results of the comparison for roll and pitch is shown in figures 6.20 to 6.21. The comparison for the roll is very good and the roll for PHINS1 is almost identical to PHINS4. The comparison for pitch is also good, but some minor differences are seen for smaller pitch motions. Another check can be done for the rigid body motions, by translating the heave from one sensor to the other. This should give the same results. The heave at PHINS 1 is translated to PHINS 4 using rigid body motions. The results are shown in figure 6.22. The motions look very much alike, and justify the assumption of rigid body motions.

Translate heave to Central Reference Point

The Time series is translated to the CRP. This is done so it can be compared to the predicted vessel motions, which are predicted for the CRP, which is close to the centre of gravity. For this translation the assumption is used that the vessel behaves as a rigid body.

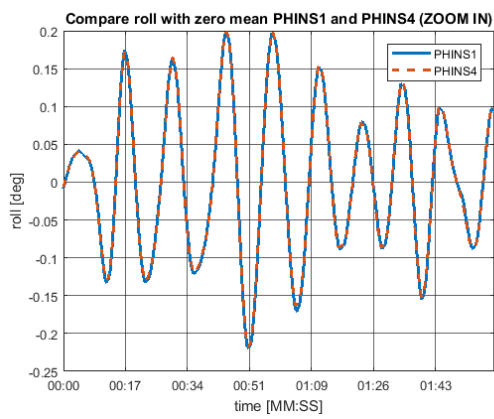


Figure 6.20: Comparison of roll measurement for sensors PHINS 1 and PHINS 4, interpolated for constant time step and with the moving average removed. The two sensors show good comparison

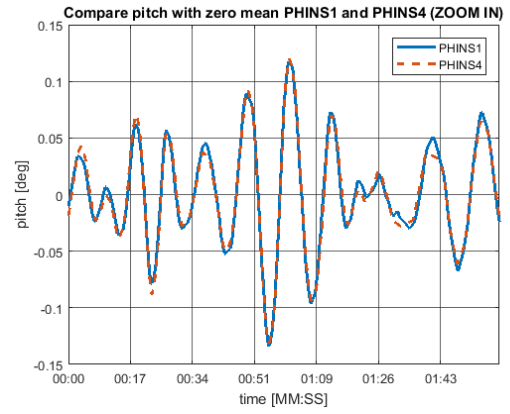


Figure 6.21: Comparison of pitch measurement for sensors PHINS 1 and PHINS 4, interpolated for constant time step and with the moving average removed. The two sensors show reasonable comparison

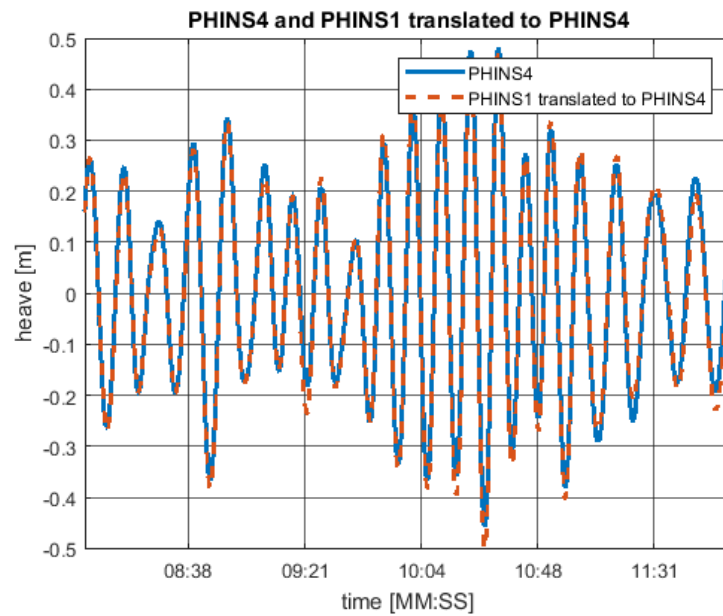


Figure 6.22: Heave motion of PHINS 1 translated to PHINS 4 and PHINS 4, showing a good comparison

7

Test Results

In this chapter, the results of predicted vessel motions are compared to measured vessel motions. The comparison is done between predicted and measured results, as shown in figure 7.1.

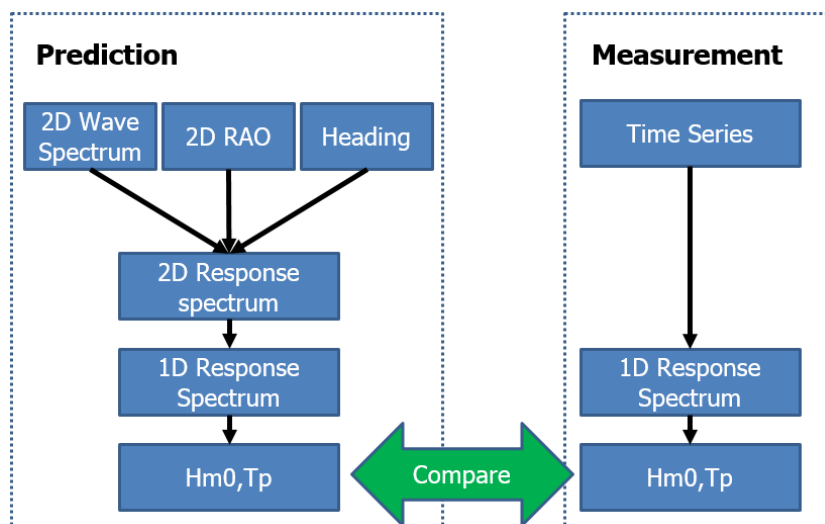


Figure 7.1: Comparison approach, the significant double amplitude SDA and peak period T_p from prediction and measurement are compared.

Four parameters are compared for the motions of the *Pioneering Spirit*. These are:

- heave at sensor location
- heave at CRP
- roll
- pitch

The prediction for heave roll and pitch is done for the vessel's CRP. The measurement is done at a sensor location, which is not at the CRP. Because the assumption of rigid body motions is used, roll and pitch are assumed independent of the location on the ship. To obtain the predicted heave motions at the sensor location, the heave at CRP needs to be translated to the sensor location, using predicted roll and pitch. To obtain the 'measured' heave motion at the CRP, the measured heave at the sensor location needs to be translated, using the measured roll and pitch. First of all, the significant double amplitude of the motions SDA, and the peak period T_p will be compared. It should be noted that due to the limited frequencies in the available wave spectrum, the peak period can only have limited values, corresponding to the available frequencies in the wave spectrum. The measured peak period also can only have limited values, this is limited by the number of samples that are used in the Fourier Transform, and the sampling rate at which the time series is sampled. Using more samples for the Fourier transform, leads to larger steps between two possible values of the T_p .

7.1. Definition of good comparison

The definition of a good comparison between measured and predicted vessel motions is based on the following criteria:

- **Minimum SDA:** Measured value of SDA should at least have a certain threshold value. For measurements with too low SDA, noise effect may become too dominant.
- **Absolute error SDA:** error between Measured SDA and predicted SDA $abs(measured - predicted)$ should not exceed a certain value. Too large difference means something is wrong either in prediction or measurement.
- **Absolute error Tp:** error between Measured SDA and predicted SDA $abs(measured - predicted)$ should not exceed a certain value, to be qualified as a good prediction

Based on the accuracy of the MRU, the minimum value of the significant double amplitude is calculated. These are shown in table 7.1.

Table 7.1: Invalid measurements due to too low SDA value

Parameter	minimum SDA	Total number of Measurements	Number of measurements with SDA too small	valid measurements
Heave at CRP	10 cm	192	95	97
Heave at PHINS4	5 cm	192	1	191
Roll	0.02 deg	192	1	191
Pitch	0.02 deg	192	3	189

7.2. Help for reading figures

The figures in this chapter show the results of the predictions compared to measurements. The terms used in the figures are explained here shortly.

Samples fft

For the measured motion - The amount of samples used in the Fast Fourier Transform (FFT) of the signal. Each point in the graph is deduced from a half hour time series. for reliability, this half hour time series is cut into a number of time samples (samples fft) of equal length. This was discussed in chapter 4.

Sensor

The name of the sensor, a MRU, that is used for the measurement of the time series. The heading of these measurements is used for the vessel motion predictions. Example sensor name: PHINS1.

RAO

The RAO is calculated by the hydrodynamic software package Ansys AQWA. Input for the calculation are among others the water depth and vessel draught. These values can be read from the name of the RAO. for example, the RAO: PS_WIDE_T20M_WD27MLINE.LIS is calculated based on a draught (T) of 20 m, and a water depth (WD) of 27 m.

Absolute error

The absolute error is calculated as:

$$\text{absolute error} = x_{\text{predicted}} - x_{\text{measured}} \quad (7.1)$$

In which x can be the significant double amplitude of the motion SDA or the peak period T_p .

7.3. Results Offshore Acceptancy Test 1

The results of the comparison between measured and predicted vessel motions are shown in this section. The wave spectrum specifics are shown in figure 7.2. The predictions are based on the RAO for a draught of 20 m and a water depth of 27 m. From the graphs, research questions are formulated at the end of this section which will be further investigated.

Environmental conditions

The environmental conditions are shown in figure 7.2. The figure shows the incoming peak wave direction in the top plot, which takes into account the vessel heading. The middle plot shows the H_{m0} of the wave spectrum, for the one dimensional wave spectrum (summed over all directions). The bottom plot shows the peak period of the one dimensional wave spectrum. The following can be seen from the plots in the figure:

- The incoming peak wave direction is around 200 degrees for the first part, until the end of 10-08. then the incoming wave direction changes rapidly. This sudden change is caused by the vessel turning 360 degrees, as part of the offshore trials. The sudden changes on 11-08 are caused by the double peakedness of the spectrum. Two peak are present at different directions. The incoming wave direction is based on only one of the two peaks, whichever is largest for the given moment.
- The significant wave height H_{m0} is increasing from 1.5 to 2.5 m on day 09-10. The wave height stays around this value for about one day and then decreases to 1.7 m at the end of day 10-08. then it stays at this value and decreases finally to around 1 m on day 12-08. Thus the highest values are measured at the beginning of the time interval.
- The peak period of the time series fluctuates strongly, with values between 5 and 11 seconds. The peak period can only take on a limited amount of values, because the wave spectrum is defined at a limited amount of frequencies. The peak period is larger for the first two days (09-08 and 10-08) and then decreases. The trend of the peak period more or less follows the trend of the significant wave height.

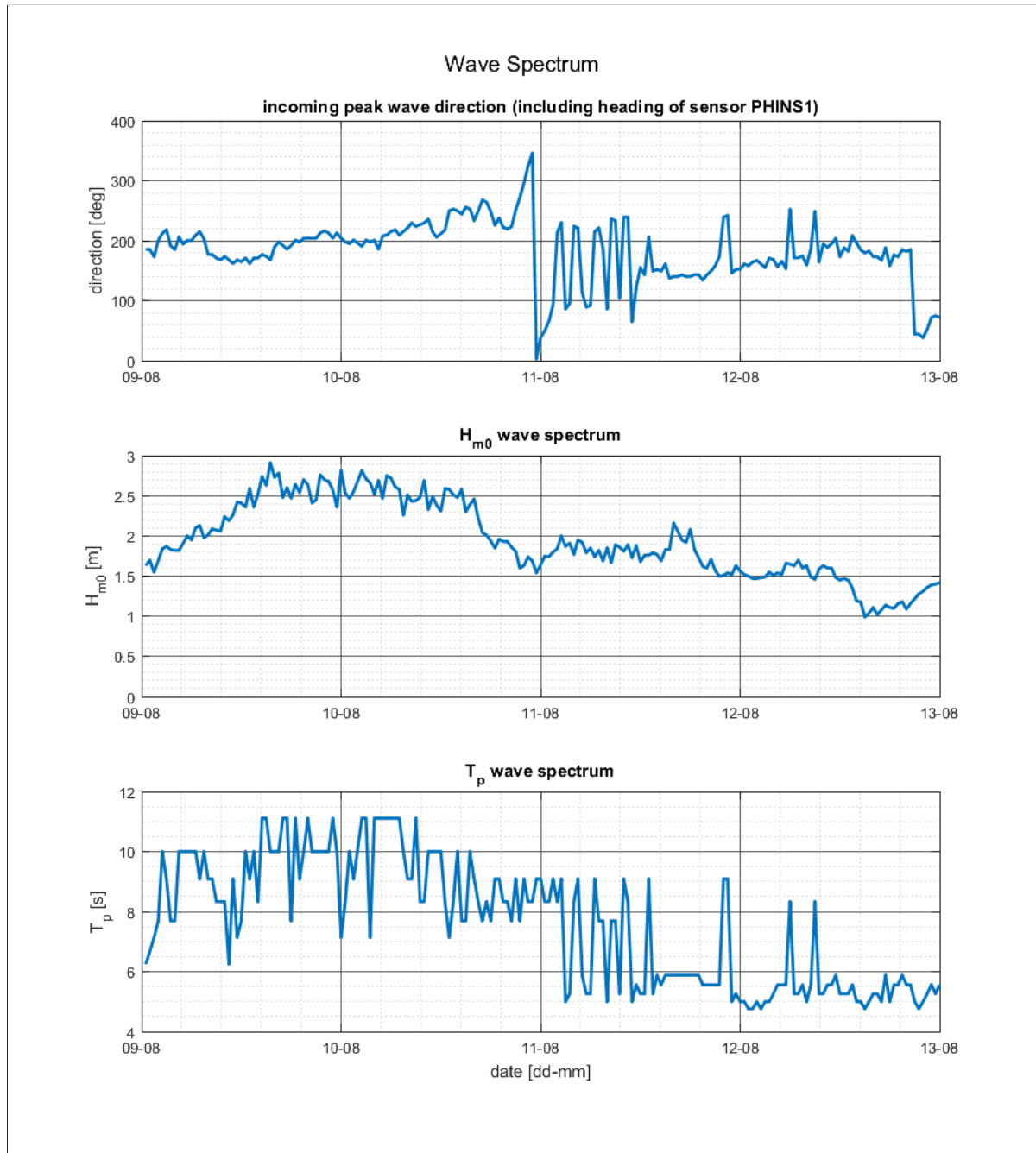


Figure 7.2: Specifics of the wave spectrum during OAT1. The figure shows the incoming wave peak wave direction (top figure), which is the peak wave direction of the waves minus the heading of the vessel. The middle figure shows the significant wave height calculated from the wave spectrum, and the bottom figure shows the peak period derived from the wave spectrum.

Roll

For the comparison between the predicted and the measured roll motion, the limits defining a good comparison are given in table 7.2. The reason for a wrong prediction, as well as the amount of good predictions, can be found in table 7.3. Figure 7.3 shows the SDA and T_p for the measured and predicted roll motion. For both these parameters, the absolute error is also plotted. Looking at the plots, the following statements can be made:

- The SDA is increasing from approximately 0.1 deg at 09-08 to 0.3 deg on 10-08. There is a large peak in the measured SDA on 10-08. Starting from 11-08, the SDA becomes rather small, with values of 0.1 deg and less.
- The SDA is over predicted at some times, and under predicted at other times, but for most of the points the roll is under predicted.
- Around half the day on 10-08, there is a high peak in the measured roll motion, this peak is not seen in the prediction.
- The T_p varies between 9 and 14 seconds. As the SDA is larger, the T_p is generally larger as well.
- The T_p exceeds the absolute error of 0.5 s for most of the time. The T_p can both be over estimated and underestimated.

Table 7.2: Parameters used for determining whether a prediction is good or not, for the roll motions. Including an explanation for the chosen values

Parameter	Value	Units	explanation
Minimum SDA	0.02	Deg	The error of the MRU for the roll is 0.01 deg RMS. This means 95 % of the measurements have an error smaller than twice 0.01 deg, see formula 6.3.
Absolute error SDA	0.02	Deg	The error of the MRU for the roll is 0.01 deg RMS. This means 95 % of the measurements have an error smaller than twice 0.01 deg, see formula 6.3.
Absolute error T_p	0.5	s	Peak period is selected from discrete spectrum. The response spectrum has only limited frequencies in it, equal to the frequencies available in the 2D wave spectrum. The value of the absolute error takes into account that T_p can only have limited values because of this. The frequency step is fixed at 0.063 rad/s, this means that the period has an increasing step size as the period increases.

Table 7.3: Overview of number of good and wrong predictions for the roll. The table shows which parameter causes a wrong prediction.

Number of comparisons	189
Absolute error SDA within limits	94 (50%)
Absolute error T_p within limits	41 (74%)
Good comparison	23 (12%)

Comparison predicted and measured Roll motion

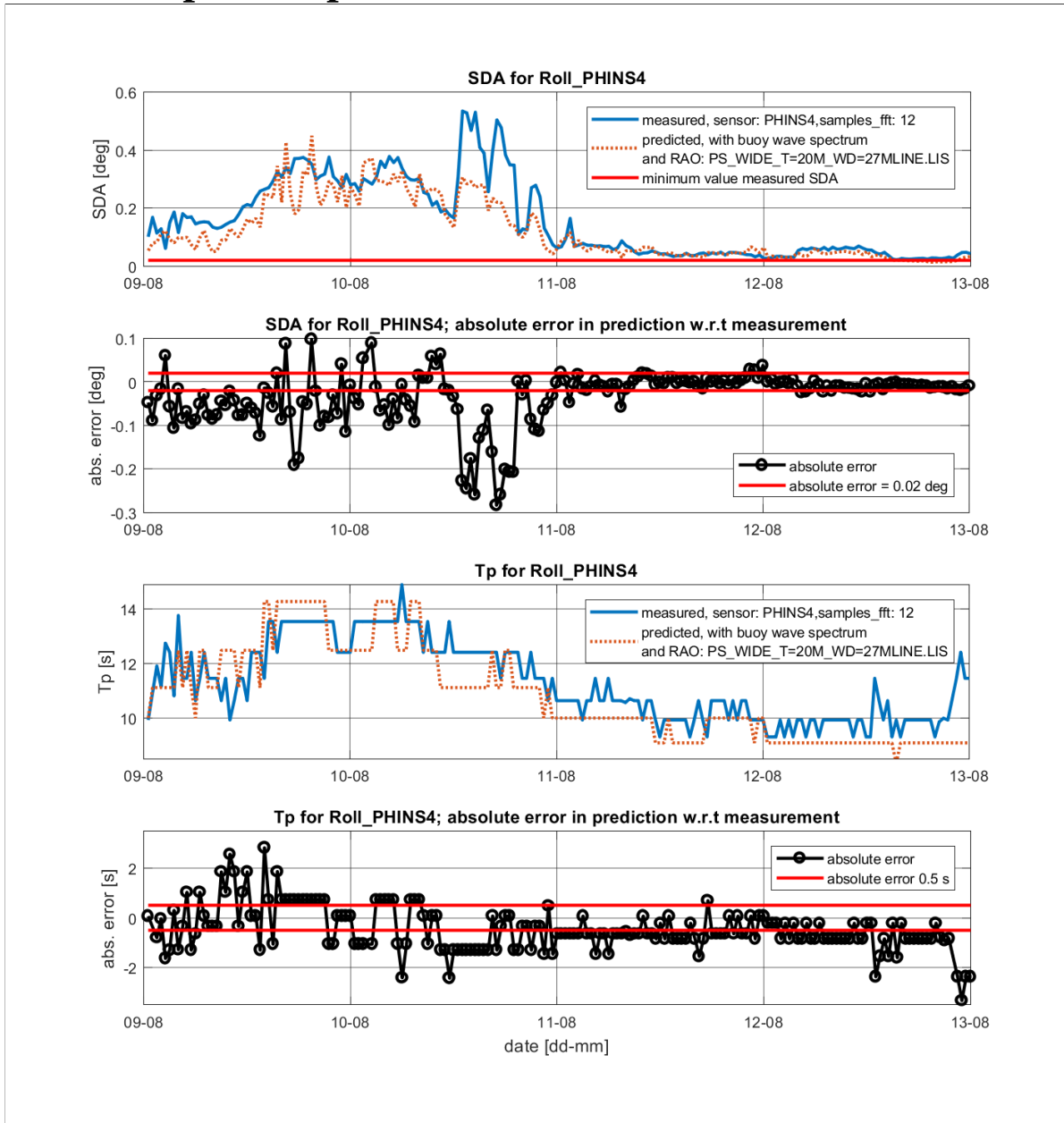


Figure 7.3: Comparison between the predicted and measured roll motion, with prediction based on a water depth of 27 m. The top plot shows the SDA, the second plot shows the absolute error between prediction and measurement. The third plot shows the T_p for both prediction and measurement, and the fourth plot shows the absolute error of the T_p .

Pitch

For the comparison between the predicted and the measured pitch motion, the limits defining a good comparison are given in table 7.4. The reason for a wrong prediction, as well as the amount of good predictions, can be found in table 7.5. Figure 7.4 shows the SDA and T_p for the measured and predicted pitch motion. For both these parameters, the absolute error is also plotted. Looking at the plots, the following statements can be made:

- The SDA of the pitch varies between 0.05 and 0.3 degrees. The largest amplitude of the roll is on 09-08 and 10-08. Starting from 11-08, the SDA is below 0.1 degrees.
- The SDA for pitch is overestimated for some time points and underestimated for other time points.
- Around half the day on 10-08, when the measured pitch is still high, the predicted pitch decreases, and is under predicted and the absolute error exceeds the minimum.
- The T_p varies between 9 and 13 seconds. As the SDA is larger, the T_p is generally larger as well.
- The T_p is over predicted and exceeds the limits of the absolute error for the first part of the time. Then starting on 10-08, the T_p is underestimated, again exceeding the absolute error. The T_p is outside the limits for most of the time.
- Only 5% of the predictions can be qualified as good, the most errors are caused by a wrong prediction of the peak period, only for 18% of the data points the T_p was correctly predicted. The SDA is good predicted for 35% of the data points.

Table 7.4: Parameters used for determining whether a prediction is good or not, for the pitch motions. Including an explanation for the chosen values

Parameter	Value	Units	explanation
Minimum SDA	0.02	Deg	The error of the MRU for the pitch is 0.01 deg RMS. This means 95 % of the measurements have an error smaller than twice 0.01 deg, see formula 6.3.
Absolute error SDA	0.02	Deg	The error of the MRU for the pitch is 0.01 deg RMS. This means 95 % of the measurements have an error smaller than twice 0.01 deg, see formula 6.3.
Absolute error T_p	0.5	s	Peak period is selected from discrete spectrum. The response spectrum has only limited frequencies in it, equal to the frequencies available in the 2D wave spectrum. The value of the absolute error takes into account that T_p can only have limited values because of this. The frequency step is fixed at 0.063 rad/s, this means that the period has an increasing step size as the period increases.

Table 7.5: Overview of number of good and wrong predictions for the pitch motion. The table shows which parameter causes a wrong prediction.

Number of comparisons	189
Absolute error SDA within limits	67(35%)
Absolute error T_p within limits	34(18%)
Total good comparisons	9(5%)

Comparison predicted and measured Pitch motion

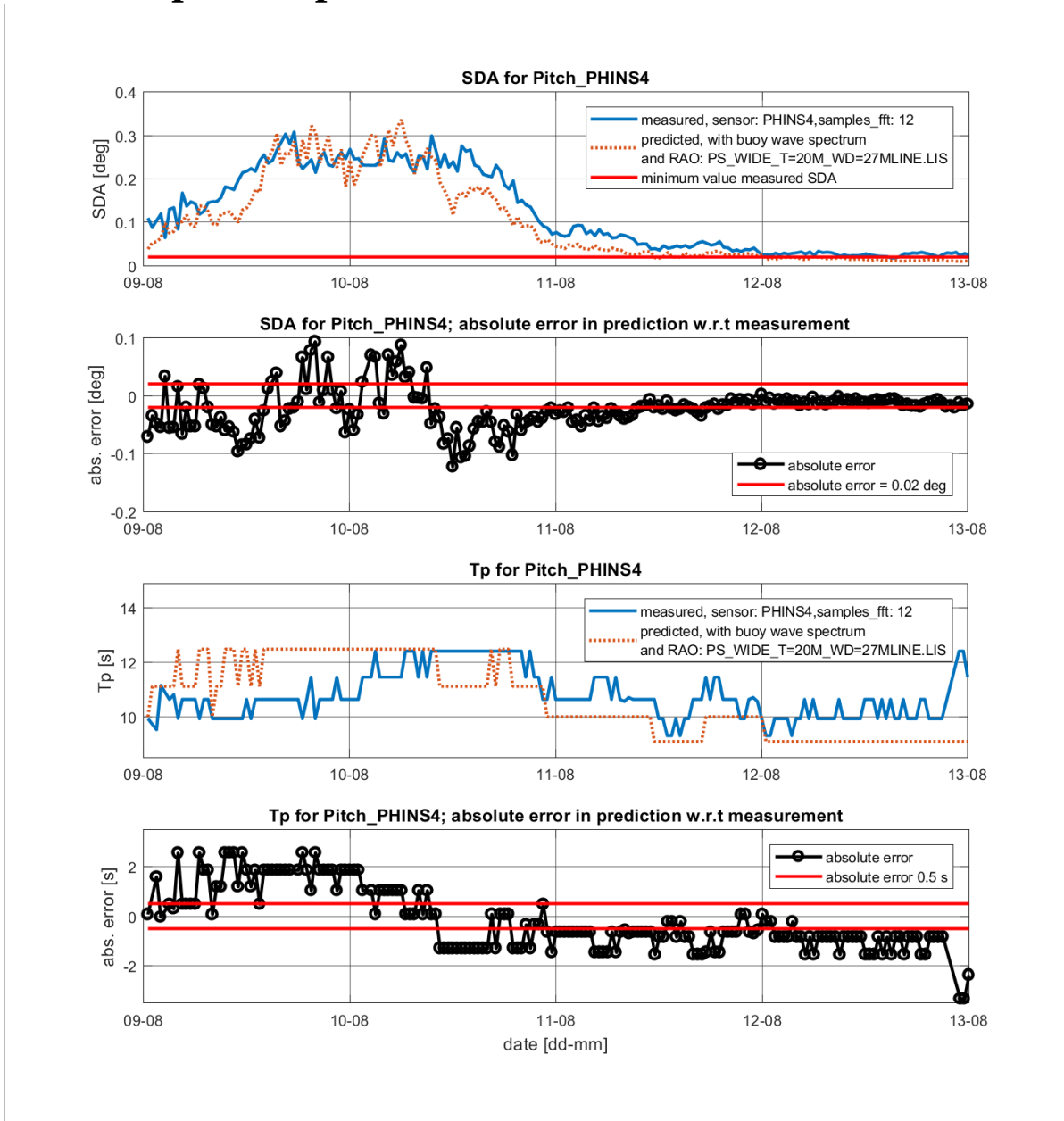


Figure 7.4: Comparison between the predicted and measured pitch motion, with prediction based on a water depth of 27 m. The top plot shows the SDA, the second plot shows the absolute error between prediction and measurement. The third plot shows the T_p for both prediction and measurement, and the fourth plot shows the absolute error of the T_p .

Heave at sensor location

For the comparison between the predicted and the measured heave motion at sensor MRU PHINS4, the limits defining a good comparison are given in table 7.6. The reason for a wrong prediction, as well as the amount of good predictions, can be found in table 7.7. Figure 7.5 shows the SDA and T_p for the measured and predicted heave motion. For both these parameters, the absolute error is also plotted. Looking at the plots, the following statements can be made:

- The measured SDA is largest in the first part of the time series, from 09-08 to 11-08, with values around 0.8 m. Starting from 11-08 to 13-08, the SDA becomes small, with values below 0.2 m.
- The SDA for predicted heave motion is underestimated for almost the entire time frame.
- The prediction is closer to the measured motions around 08-10, where it falls within the limits of the absolute error for most of the data points. This is the time where the SDA is highest.
- The measured T_p is largest on 10-08, around 12 s, and smaller for 09-08 and 11-08 until 13-08 with values of 10-11 s.
- The peak period T_p is overestimated on 09-08 by more than 10 %. At the start of 10-08, the predicted T_p agrees well with the measured one later on the day, the T_p is underestimated, varying above and below the absolute error limits.
- There is a time at 10-08 where both SDA and T_p are predicted correctly, however, good prediction of SDA is no guarantee for a good prediction of T_p and vice versa.
- Both the SDA and T_p are predicted in a good way 66 % of the time intervals. The total good predictions, are only 5 % of the total.

Table 7.6: Parameters used for determining whether a prediction is good or not, for the heave at sensor location MRU PHINS4. Including an explanation for the chosen values

Parameter	Value	Units	explanation
Minimum SDA	0.05	m	The error of the MRU for the heave is 2.5 cm or 2.5% RMS. This means 95 % of the measurements have an error smaller than twice the RMS, see formula 6.3.
Absolute error SDA	0.05	m	The error of the MRU for the pitch is 0.01 deg RMS. This means 95 % of the measurements have an error smaller than twice 0.01 deg, see formula 6.3.
Absolute error T_p	0.5	s	Peak period is selected from discrete spectrum. The response spectrum has only limited frequencies in it, equal to the frequencies available in the 2D wave spectrum. The value of the absolute error takes into account that T_p can only have limited values because of this. The frequency step is fixed at 0.063 rad/s, this means that the period has an increasing step size as the period increases.

Table 7.7: Overview of number of good and wrong predictions for the heave at sensor location, MRU PHINS4. The table shows which parameter causes a wrong prediction.

Number of comparisons	191
Absolute error SDA within limits	127(66%)
Absolute error T_p within limits	126(66%)
Total good comparisons	9(5%)

Comparison predicted and measured Heave motion at PHINS4

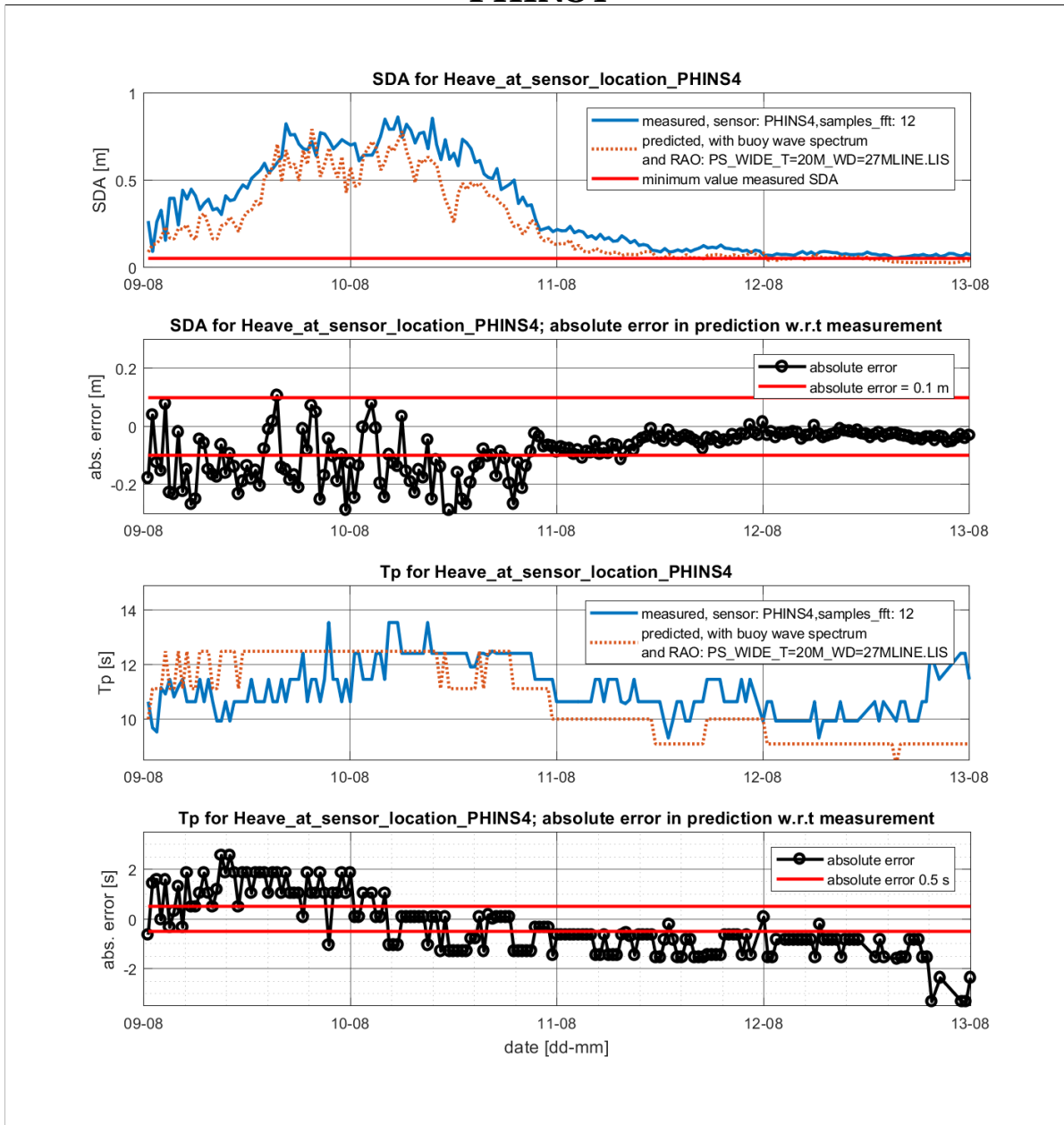
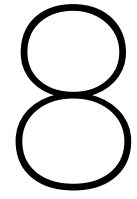


Figure 7.5: Comparison between the predicted and measured heave motion at sensor location PHINS4, with prediction based on a water depth of 27 m. The top plot shows the SDA, the second plot shows the absolute error between prediction and measurement. The third plot shows the T_p for both prediction and measurement, and the fourth plot shows the absolute error of the T_p .

Research questions based on results

Based on the results, the following questions arise:

- How does the prediction change for RAO based on different water depths?
- What is the cause of the peak in the measured SDA for the Roll at the end of day 10-08, and why is there a sudden large difference between prediction and measurement, what changes in the conditions during the day on 10-08? See figure 7.3.
- What is the cause of the peak in the measured SDA for the Pitch at the end of day 10-08, and why is there a sudden large difference between prediction and measurement, what changes in the conditions during the day on 10-08?
- What is the contribution to the heave at the bow in terms of heave at CRP, roll and pitch?
- What is the relation between the amplitude of the measured and predicted SDA for heave, roll and pitch?



Discussion of Results

In chapter 7, the results lead to questions, which will be further investigated here.

8.1. Contribution of heave at CRP, roll and pitch to predicted heave

The heave at the location of the MRU's is constructed from the heave, the roll and the pitch, using rigid body motions. This is explained in section 6.3. The total heave for MRU PHINS1 and PHINS4 are split in these contributions. The result is shown for PHINS1 and PHINS4 in figures 8.1 and 8.2. Looking at the two plots, it can be seen that the predicted motions for the total heave at PHINS1 is larger than for PHINS4. The heave at the CRP is the same for PHINS1 and PHINS4. Because the total heave motion for PHINS4 is smaller than for PHINS1, the relative contribution of the heave at the CRP is larger. The percentage of the contribution to the total heave at the location of the MRU is given in table 8.1. The same is true for the roll. PHINS1 and PHINS4 are placed at the same distance from the CRP in the y-direction, see figure 6.14. Because the distance in y-direction from the MRU to the CRP is equal for PHINS1 and PHINS4, the amplitude of the roll contribution is the same for the two MRUs, and the relative contribution of the roll is larger for PHINS4 than for PHINS1. The amplitude of pitch contribution is larger for PHINS1 than PHINS4.

Table 8.1: Contribution of different motions to the total heave motions at MRU PHINS1 and PHINS4. The contribution of the pitch is largest for both PHINS1 and PHINS4. For PHINS1, the contribution of the pitch towards the total response is larger for PHINS1 than for PHINS4.

contribution to total heave response SDA		
	PHINS1	PHINS4
contribution heave at CRP	18.00%	30.00%
contribution roll	14.00%	23.00%
contribution pitch	68.00%	47.00%
contribution total	100.00%	100.00%

conclusions

The predicted heave motion at the location of the MRUs is dominated by the pitch motion. For PHINS4, the pitch contributes 47% towards the total response, and for PHINS1, the pitch contributes 68% towards the total response. This means that a change in the pitch prediction will have a large effect on the total prediction for the heave at the locations of the MRU. The influence of a change in the pitch prediction will be larger for PHINS1 than for PHINS4. In general, the change of pitch motions will contribute more to the heave as the distance in the x-direction from the CRP increases.

The absolute values of the contribution of the heave at CRP, and the roll toward the total response, are the same for MRU PHINS1 and PHINS4.

The contribution of the heave at CRP and the roll, on the total heave response is smaller than the pitch, but still significant, with relative contributions between 14 and 30%.

Although the contribution of the pitch is largest, this does not necessarily mean that the pitch prediction causes the large differences in the prediction and the response. If for example the roll is underestimated, its true contribution towards the total heave motion at the bow would be larger than is assumed here.

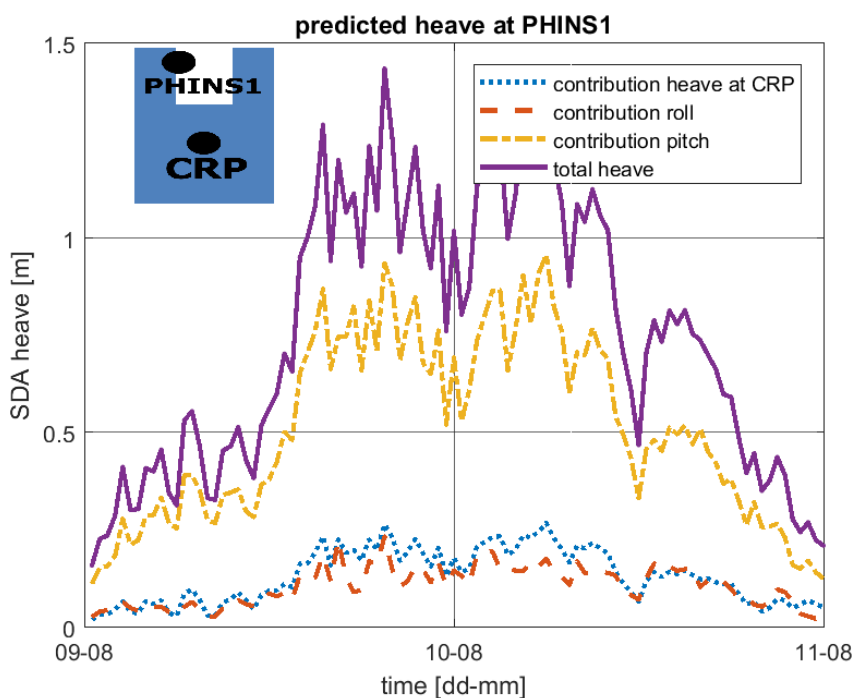


Figure 8.1: Predicted heave motion at location of MRU PHINS1. The heave motion is consist of a contribution due to heave motion at the Central Reference Point (CRP), a contribution due to the roll, and a contribution due to the pitch motions. The contribution of the pitch motion is largest, and has the largest contribution to the total response for the heave at PHINS1. The contributions of the heave at CRP and the roll are the same order of magnitude.

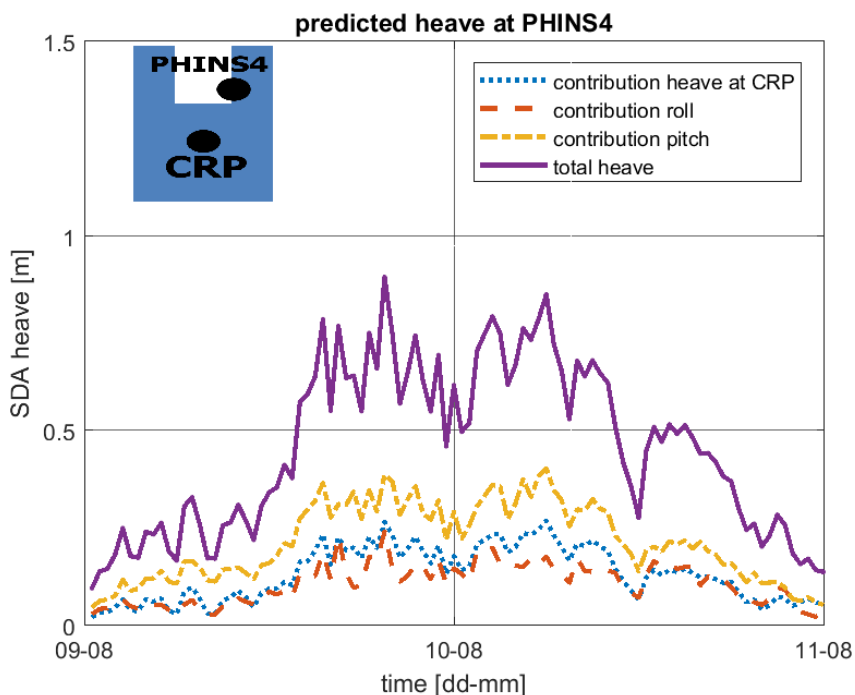


Figure 8.2: Predicted heave motion at location of MRU PHINS4. The heave motion is consist of a contribution due to heave motion at the Central Reference Point (CRP), a contribution due to the roll, and a contribution to the pitch. The contributions of the heave at CRP, roll and pitch are in the same order of magnitude, the contribution of the pitch motion is largest.

8.2. Influence of motion amplitude on quality of prediction

The amplitude of the measured motions varies over time. In this section, the influence of the amplitude of the SDA on the quality of the predictions is investigated. To give insight in the influence of the amplitude of the SDA on the prediction, the SDA of the predicted motions is plotted against the amplitude of the measurements. To see how the quality of the prediction changes with amplitude, the heave at location of the MRU, the roll and pitch are compared for different minimum values of the SDA.

Table 8.2: Comparison of the number of good predictions for different minimum values of the SDA.

Parameter	minimum SDA	# of comparisons	# of good comparisons	percentage
Heave at PHINS4	0.1 m	128	63	49%
	0.4 m	69	18	26%
Heave at PHINS1	0.1 m	183	99	54%
	0.4 m	89	22	25%
Roll PHINS1	0.02 deg	184	84	46%
	0.15 deg	83	6	7%
Pitch PHINS1	0.02 deg	186	75	40%
	0.15 deg	69	13	19%

conclusions

The quality of the prediction is especially good in the low amplitude region. This is true for the heave at MRU locations, for roll and pitch.

An increase of the minimum SDA that is valid, causes a lower percentage of good predictions. This is true for the roll, the pitch and the heave at PHINS1 and PHINS4.

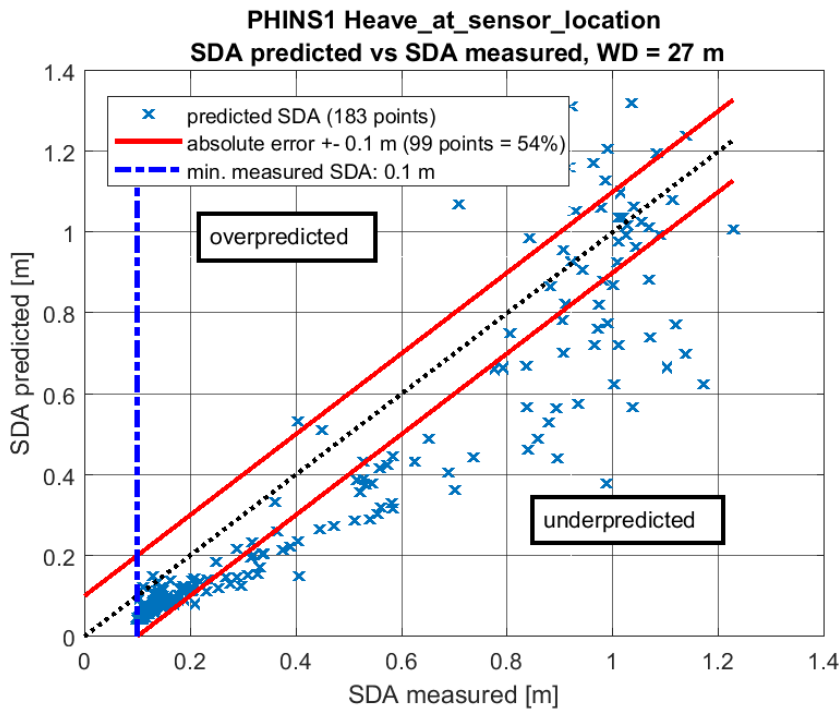


Figure 8.3: The predicted SDA of the heave at the sensor location plotted against the measured SDA.

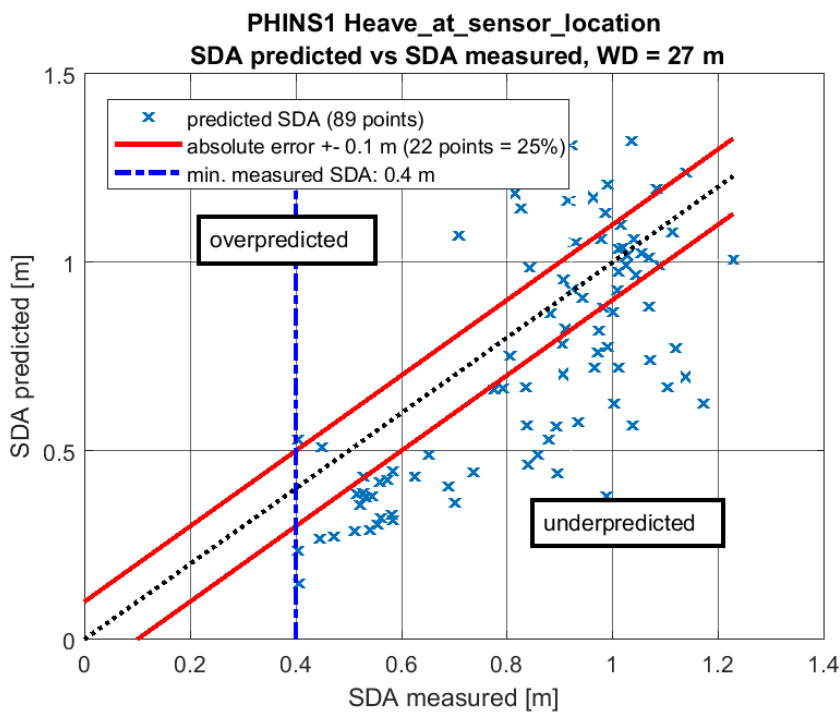


Figure 8.4: The predicted SDA of the heave at sensor location plotted against the measured SDA.

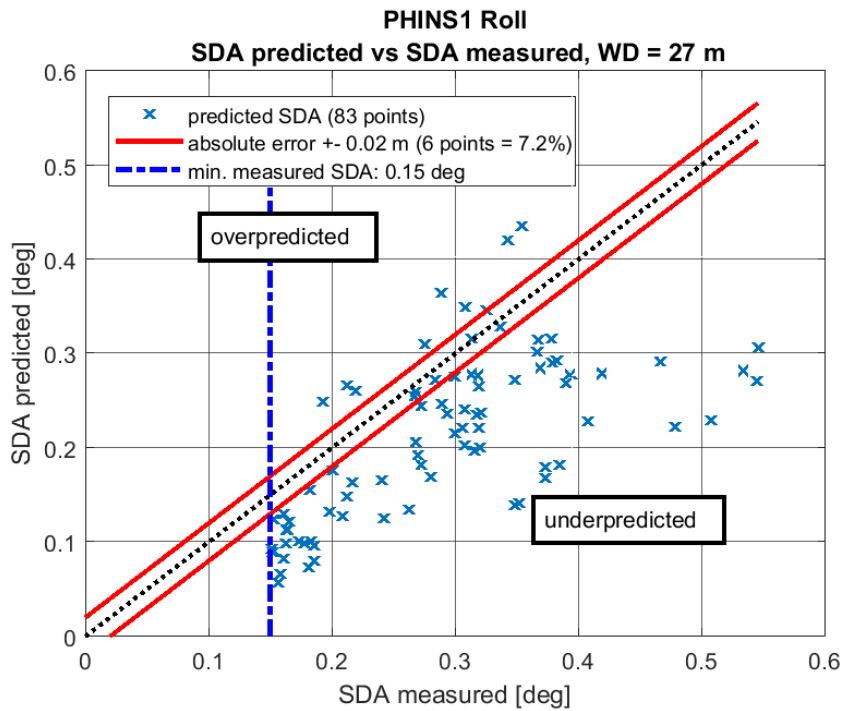


Figure 8.5: The predicted SDA of the roll plotted against the measured SDA.

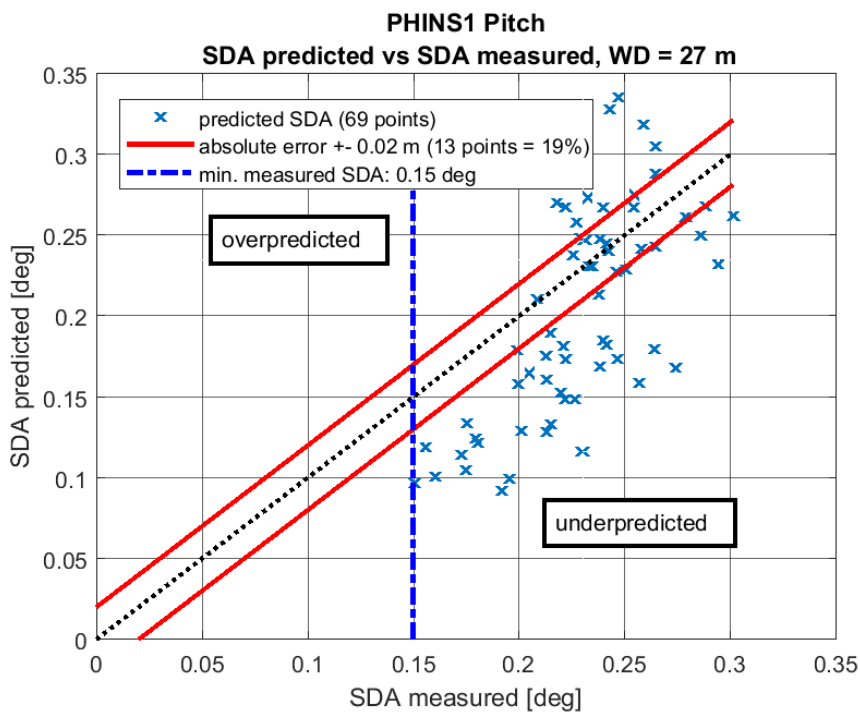


Figure 8.6: The predicted SDA of the roll plotted against the measured SDA.

8.3. Prediction for different water depths

The predictions done in the previous section in general do not show a good comparison with the measured motions. In this section, the RAO is calculated based on different water depths, to see if this can improve the predictions. Tables 8.3, 8.4 and 8.5 show the influence of a changing water depth on the prediction of the motions. For the roll, the prediction is best at a water depth of 27 and 35 m water depth. For the pitch, the prediction improves significantly if the water depth in the prediction is changes from 27 to 35 m. The good predictions increase from 5 to 17%. For the heave at the sensor location, the prediction is also improving for a water depth of 35 m compared to 27 m. The amount of good predictions increases from 5% to 16 %.

Roll

Table 8.3: Overview of number of good predictions for the roll for predictions based on different water depths. The table shows the good predictions for the SDA and T_p separately and for the SDA and T_p combined.

Water depth of RAO	26 m	27 m	35 m	1000 m
Absolute error SDA within limits	85(45%)	97(51%)	87 (46%)	67(35%)
Absolute error T_p within limits	49(26%)	50(26%)	58(30%)	58(30%)
Total good comparisons	20(10%)	23(12%)	23(12%)	20(10%)

pitch

Table 8.4: Overview of number of good predictions for the pitch for predictions based on different water depths. The table shows the good predictions for the SDA and T_p separately and for the SDA and T_p combined.

Water depth of RAO	26 m	27 m	35 m	1000 m
Absolute error SDA within limits	76(40%)	79 (41%)	130 (68%)	105 (55%)
Absolute error T_p within limits	41(21%)	36 (19%)	60 (31%)	26 (14%)
Total good comparisons	9(5%)	9(5%)	33(17%)	10 (5%)

Heave at sensor location

Table 8.5: Overview of number of good predictions for the heave at location of sensor MRU PHINS4 for predictions based on different water depths. The table shows the good predictions for the SDA and T_p separately and for the SDA and T_p combined.

Water depth of RAO	26 m	27 m	35 m	1000 m
Absolute error SDA within limits	116(61%)	126(66%)	157(82%)	133(70%)
Absolute error T_p within limits	95(50%)	96(50%)	111(58%)	86(43%)
Total good comparisons	6(3%)	9(5%)	31(16%)	8(4%)

The following can be concluded from the comparisons with different water depths:

- For the Roll the predictions are best for an RAO based on 27 or 35 m water depth.
- For the Pitch the predictions are best for an RAO based on 35 m water depth.
- For the Heave at CRP the predictions are best for an RAO based on deep water.

The comparison of RAOs described in chapter 6, showed the RAO shifts towards higher frequencies as the water depth increases. Comparing the situation for 27 and 35 m of water depth, and knowing the RAO is (among others) based on the added mass added damping and incoming wave force, the following is found:

- Added mass for 35 m is smaller than for 27 m
- Added damping is smaller for 35 m than for 27 m
- The incoming wave force is almost the same for a water depth of 35 and 27 m
- The mass of the vessel remains the same for the different water depths
- The static buoyant force on the vessel remains the same for different water depth

This means that decreasing the added mass and/or added damping, can give a better prediction.

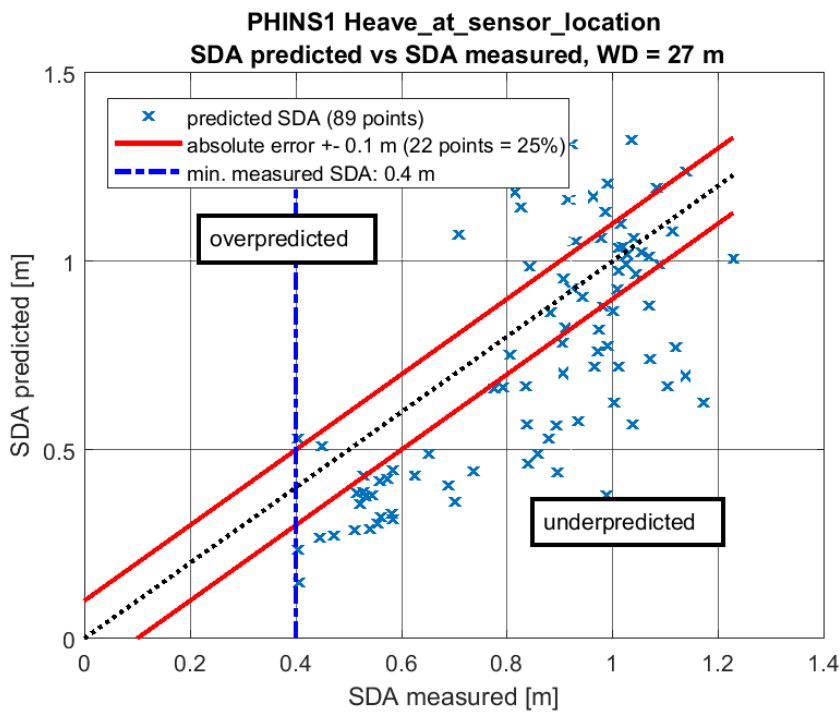


Figure 8.7: Heave measured at sensor location, for MRU PHINS1. The predicted SDA is plotted against the measured SDA. The prediction is based on an RAO of 27 m water depth. Most of the motions are underpredicted, especially if the measured SDA is low (0.4 to 0.8 m). For a larger measured SDA, there is a wider spread in the prediction, and the SDA is not always underpredicted, but can even be over predicted.

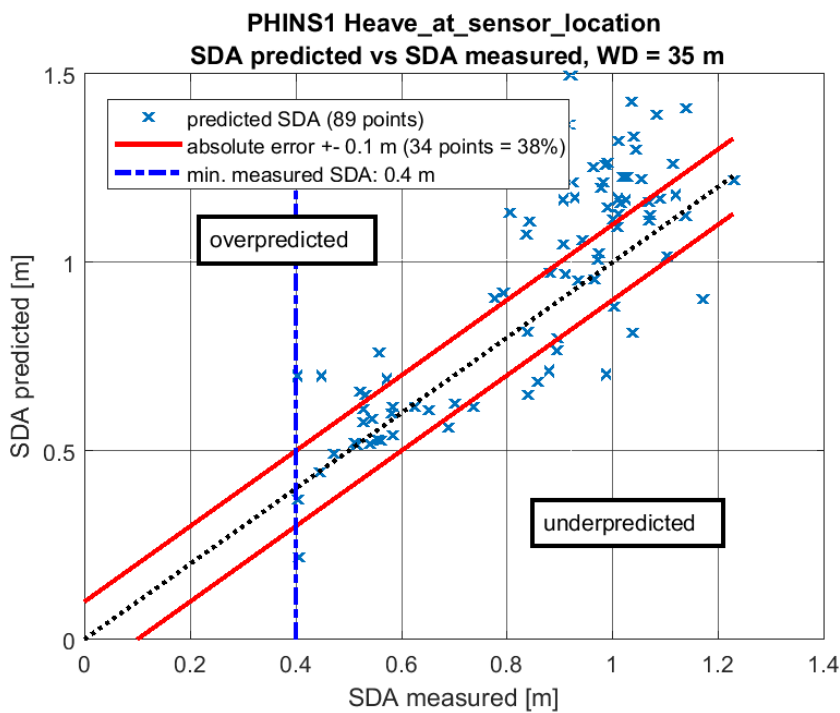


Figure 8.8: Heave measured at sensor location, for MRU PHINS1. The predicted SDA is plotted against the measured SDA. The prediction is based on an RAO of 35 m water depth. For low measurements (0.4 to 0.8 m), the good predicted, within the 0.1 m error limits. For measurements, the SDA is mostly over predicted.

8.4. peak in roll motion

The peak in the roll motion present in figure 7.3 is discussed here. A zoom in on the area where the peak occurs, is shown in figure 8.9, together with the incoming wave direction. It can be seen that the large peak in the measured roll motion is occurring as the incoming peak wave direction increases above around 220 degrees. The prediction does not follow the measured motion for these points. The predicted roll motion is underestimated for a in incoming wave direction of more than 220 degrees.

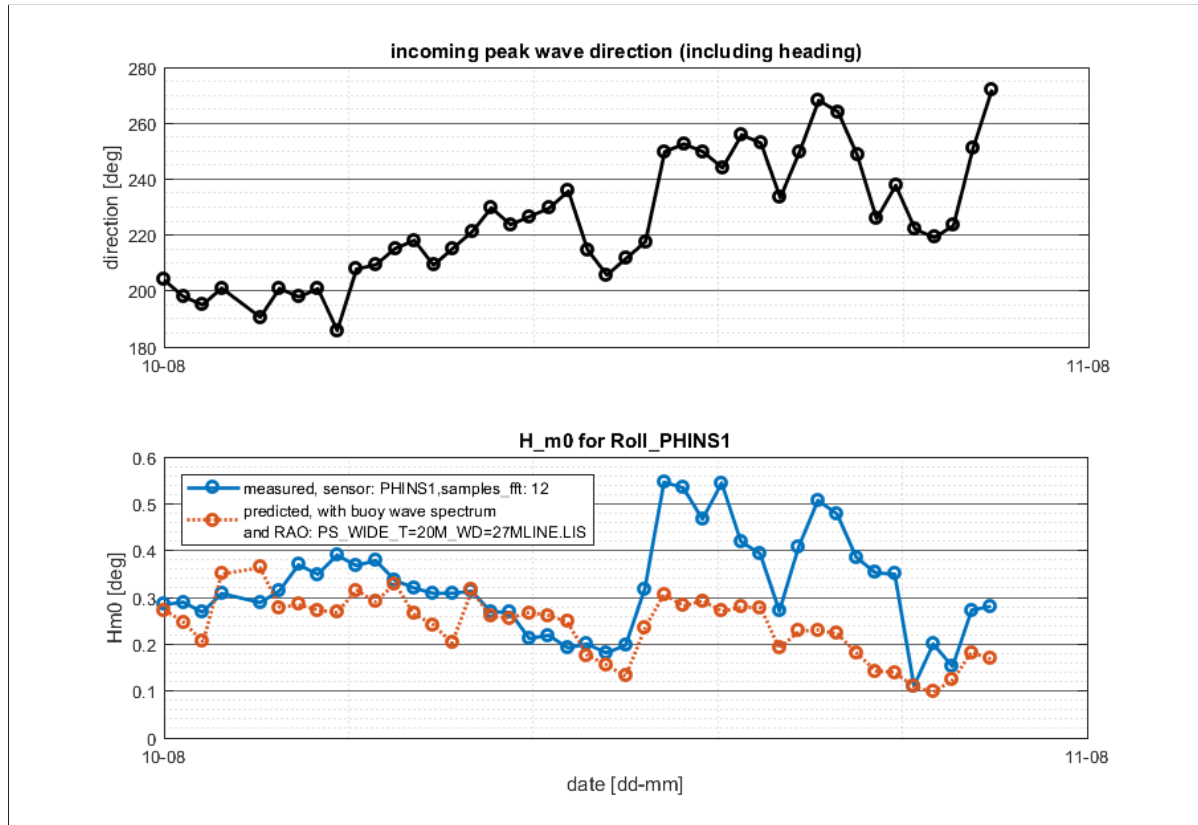


Figure 8.9: incoming wave direction (top) and comparison between measurement and prediction (bottom). for day 10-08. When the direction of the incoming wave increases to 240 degrees or above, the predicted and measured response deviate strongly. The measured SDA reacts stronger to a change in the wave direction than the predicted SDA. The prediction is worse for waves coming from the side, compared to waves coming from behind the vessel.

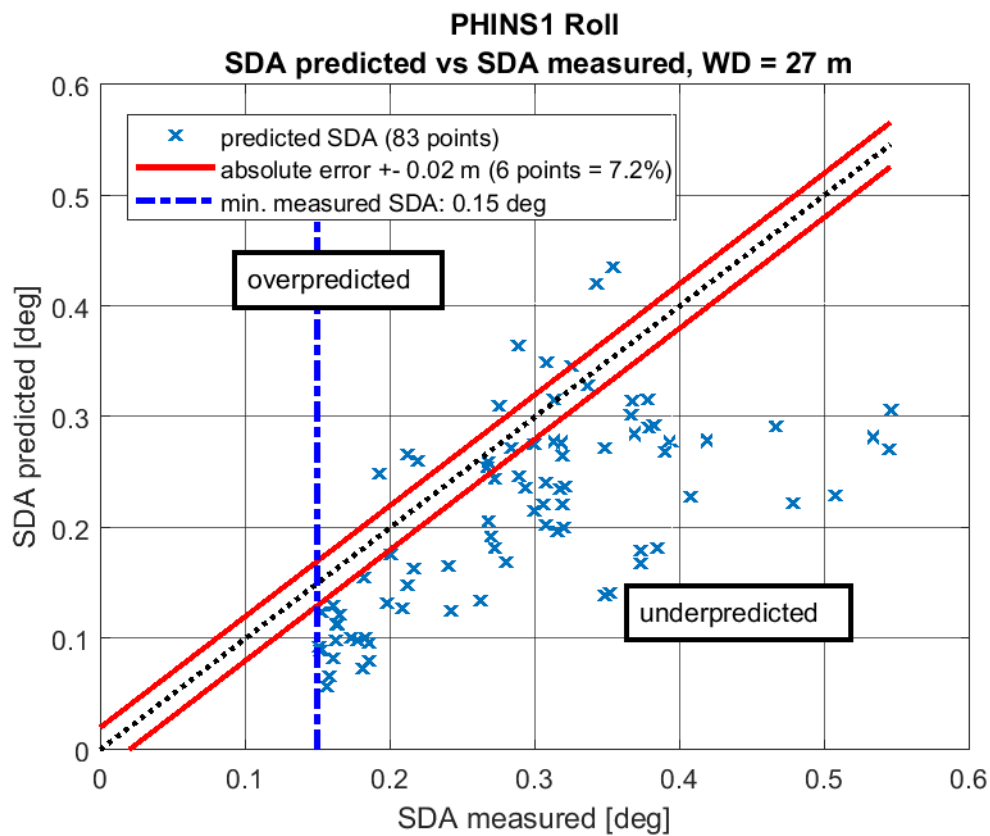


Figure 8.10: Predicted SDA plotted against the measured SDA. The plot shows the dependence on the incoming wave direction. For an incoming wave direction larger than 220 degrees, the SDA is mostly under predicted for the roll motion

Conclusions and Recommendations

To quantify and reduce the uncertainty of the vessel motion prediction, the following questions need to be answered:

9.1. How do predicted vessel motions based on a measured wave spectrum compare to measured motions in shallow water?

For a water depth of 27 m, a draught of 20 m, and a wave amplitude varying between 1 and 3 m, the measured vessel motion response is compared to the predicted response. The comparison is made for the heave at the bow, the roll and pitch.

9.1.1. Heave at the bow

For heave at the bow, the predicted SDA is within a range of 10 cm from the measured value for 25% of the comparisons, see figure 8.7.

9.1.2. Roll

The predicted SDA of the roll is within 0.02 deg from the measured value for 7% of the comparisons, see figure 8.10. The roll is especially underpredicted for a peak direction between 220 and 260 degrees, see figure 8.9.

9.1.3. Pitch

The predicted SDA of the pitch is within 0.02 deg from the measured value for 19% of the comparisons, see figure 8.6.

9.1.4. Peak period

The comparison of the peak period T_p of the measured and predicted responses for heave at the bow, roll and pitch, show an error larger than 0.5 s, for most comparisons. See figures 7.3 to 7.5 This is caused by the large frequency step in the measured wave spectrum used for the prediction, which has a value of 0.063 rad/s. This means for a period of 10 s, a period step of 1,1 second. See section 6.2 and figure 6.3.

9.1.5. contribution of roll and pitch to heave at the bow

The heave at the bow is dominated by the pitch motions. The contributions of the pitch to the heave at the bow are on average 68 %. The contribution of the roll is smaller, but can have a contribution up to 30 % to the heave at the bow. See figure 8.1 and 8.2 and table 6.3.

9.1.6. Influence of motion amplitude on quality of prediction

The quality of the prediction is strongly dependent on the amplitude of the SDA. For larger values of the measured SDA, there is a larger spread in the predicted SDA. This results in a less accurate prediction of SDA for larger amplitudes. See table 8.2.

9.1.7. Prediction for different water depths

Comparing the predictions for different water depths, shows an improvement in the prediction at larger water depth for low amplitudes of the SDA, but causes an underestimation for larger SDA. See figures 8.7 and 8.7.

9.2. How do shallow water, small keel clearances and vessel shape influence the equation of motion?

Waves are influenced by the seabed for a ratio $h/\lambda < 0.5$, in which h is the water depth and λ is the wave length. Waves at a length of 54 m are influenced by the seabed, which is at a frequency of 1.1 rad/s for a regular wave. The water is said to be shallow with regard to the vessel for a depth over draught ratio of $h/T < 7$. In which h is the water depth and T is the draught of the vessel [3]. This means for the investigated situation ($h/T = 1.35$) the water is shallow with regard to the depth over draught ratio. *Pioneering Spirit* is very wide compared to the draught, when compared to other vessels. For this type of vessel shape, the potential damping is larger than for a vessel which is less wide, see figure 2.4. The small keel clearance causes an increase in added mass, and the occurrence of a cushioning and sticking effect is expected. The influence of the water depth on the RAO was investigated, and the following can be concluded:

- mass - no influence
- added mass - as the water depth decreases, this influences the added mass. The added mass is larger as the water depth decreases.
- potential damping - The potential damping is increased as the water depth decreases.
- restoring coefficient - does not change with a changing water depth or change in keel clearance.
- incoming wave forces the incoming wave force increases as the water depth increases.

So the added mass, potential damping, and Froude-Krilov forces all increase as the water depth decreases. This causes the RAO to be smaller. See section 3.8.

9.3. How large is the contribution of the individual effects towards the total response?

The increase in added mass is likely to be the most dominating effect in this respect, especially for the heave motion. The shape of the vessel is especially causing a strong influence of the added mass, see chapter 2.

9.4. What steps are taken to predict the vessel motions?

The prediction is done in the frequency domain, using a 2D frequency spectrum, 2D RAO and the measured vessel heading, see chapter 4.

9.5. Which effects are taken into account in the current approach?

The directional wave spectrum, the directional response, the heading of the vessel. The proximity of the seabed. The calculation is done based on linear theory in the frequency domain.

9.6. Which effects are not taken into account in the current approach?

The response is calculated in the frequency domain, assuming linear wave theory. The non-linear effects, cushioning and sticking, are not taken into account. Viscous damping is not taken into account.

9.7. What is the validity range of the current approach?

As the ratio of heave motion over Under Keel Clearance (UKC) increases, the cushioning and sticking contributions increases. It is expected that the overprediction of the SDA, can be caused because the cushioning and sticking effect causes a decrease in the motion amplitude. This effect is known to have a dominating effect for an amplitude over UKC of 0.5 2, which means for a UKC of 7 m, a motion amplitude of 3.5 m. Viscous damping is especially large in roll damping, the contribution of roll is relatively small, and therefore the viscous damping is not expected to give a large improvement to the predictions.

9.8. How large is the uncertainty in the current approach?

The accuracy of the 2D wave spectrum used in the prediction is 3 degrees in the angular direction. The wave spectrum has a constant frequency step of 0.063 rad/s, meaning that for higher T_p the step is larger, see figure 6.3. The uncertainty of the measurement is based on the sensor accuracy. For the heave, the accuracy is 5 cm, meaning in 95% of the cases, the measurement is within 5 cm above or below the measured value. For the roll and the pitch, the accuracy is 0.02 deg. The mesh size of the *Pioneering Spirit* is rather coarse, 2.2 m panel length. With a UKC of 7 m, there are more than 3 panel sizes between keel and sea floor. The absolute minimum is 1 panel size clearance. The time series is converted to the frequency domain, the sampling frequency determines the frequency step in the measured response spectrum, see chapter 4.

9.9. Which effects need to be adjusted/added to obtain a result that shows better comparison with the real world situation?

The large step in the wave spectrum causes a large uncertainty in the peak period. This uncertainty could be reduced by fitting a wave spectrum over the measured spectrum, or reducing the frequency step in the measured signal. The cushioning and sticking due to the proximity of the sea floor would lead to a smaller response, and could improve the comparison where the motions are overestimated. Taking into account the viscous damping would increase the damping term, and thus reduce the amplitude of the RAO.

9.10. Recommendations

9.10.1. increase precision of wave spectrum

The prediction of the peak period is limited by the precision of the buoy data. In order to do a good comparison for the peak period, the precision of the wave spectrum should be increased. This can be done by fitting the measured spectrum, or by using buoy data which has a smaller frequency step.

9.10.2. Testing with more data

The amount of data currently available is limited. If another shallow water test is investigated, with varying motion amplitudes and incoming wave directions, it could be investigated how the response is dependent on different incoming wave directions and amplitudes. Similar plots as made in figure 8.10 could be made, where the dependence on the incoming wave direction could be investigated, to see if the predictions are better or worse dependent on wave direction, and motion amplitude.

9.10.3. increase number of elements for calculation of the RAO

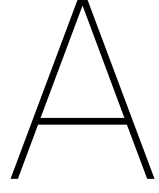
The mesh size of the *Pioneering Spirit* is rather coarse, with a 2.2 m panel length. With a UKC of 7 m, there are 3 panel sizes between keel and sea floor. The absolute minimum is 1 panel size clearance. Although this should be enough, it is advised to check if changing the panel size changes the RAO.

9.10.4. model test

A model test could be performed to validate the results that have been obtained, and spot trends for changing water depth, draught and wave spectra. Another model test could also be performed to check the influence of the cushioning and sticking effect. This test would be performed as follows: Investigate the time domain response of the vessel to a regular wave of different frequencies, for various wave amplitudes. It is expected that for a higher wave amplitude, the response becomes more non-linear as cushioning and sticking is expected to increase with increasing amplitude, as was found in [4].

9.10.5. Comparison of 3 hours maximum

The comparison here is made for the SDA and peak period. For the execution of projects offshore, it is very important to know what the maximum motion amplitude is. This can be investigated by looking at the 3 hours maximum.



Fast Fourier Transform

The FFT is used to transform time series to the frequency domain.

$$Y_{block_p}(k) = FFT\{y_{zero\ mean}\} = \sum_{j=1}^n y_{zero\ mean}(j) W_n^{(j-1)(k-1)} \quad (A.1)$$

with

$$W_n = e^{(-2\pi i)/n} \quad (A.2)$$

Where $y_{zero\ mean}$ is the signal of length n , that is transformed from time domain to frequency domain, i.e. vessel motion or wave elevation time series. The output $Y_{block}(k)$ consist of a real and an imaginary part. All p segments are combined in one Fourier matrix F , build up of k rows and P columns.

$$F = \begin{bmatrix} Y_{block_1}(1) & & & Y_{block_p}(1) \\ & \cdot & & \\ & & \cdot & \\ Y_{block_1}(k) & & & Y_{block_p}(k) \end{bmatrix} \quad (A.3)$$

The Fourier Transform matrix F is split in a real and an imaginary part.

$$R = \Re\{F\} \quad (A.4)$$

$$I = \Im\{F\} \quad (A.5)$$

$$R = \begin{bmatrix} \Re\{Y_{block_1}(1)\} & & & \Re\{Y_{block_p}(1)\} \\ & \cdot & & \\ & & \cdot & \\ \Re\{Y_{block_1}(k)\} & & & \Re\{Y_{block_p}(k)\} \end{bmatrix} \quad I = \begin{bmatrix} \Im\{Y_{block_1}(1)\} & & & \Im\{Y_{block_p}(1)\} \\ & \cdot & & \\ & & \cdot & \\ \Im\{Y_{block_1}(k)\} & & & \Im\{Y_{block_p}(k)\} \end{bmatrix} \quad (A.6)$$

From the Fourier transform, the energy density spectrum E_{block_p} for each block can be calculated.

$$E_{block_p}(f) = \frac{1}{N_{block}} \frac{1}{f_s} \sum_{i=1}^{N_{block}} R^2(i, p) + I^2(i, p) \quad (A.7)$$

Where R and I are matrices of size $N_{seg} \times p$. p is the index of the block, which is to be evaluated. By dividing the result by f_s , the spectrum becomes a function of frequency in [Hz]. The total energy is then calculated as the average of the segments.

$$E_{tot}(f) = \frac{1}{p} \sum_{i=1}^p E_{block_i}(f) \quad (A.8)$$

To transform the spectrum from [Hz] to [rad/s] the frequency vector is multiplied by 2π , and the energy density is divided by 2π . The total energy in the spectrum does not change due to this transformation.

$$E_{tot}(\omega) = \frac{E_{tot}(f)}{2\pi}; \quad \omega = 2\pi f \quad (A.9)$$

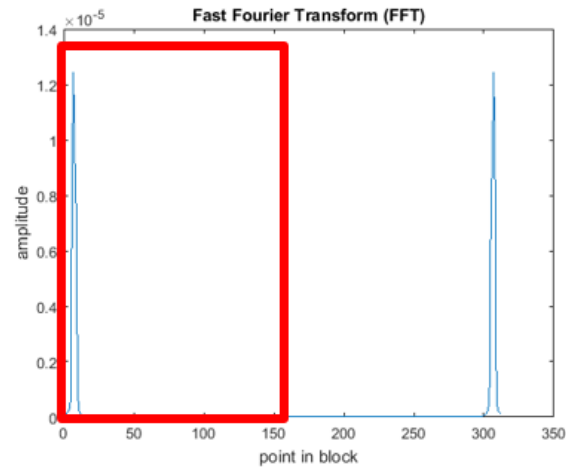


Figure A.1: Result of Fast Fourier Transform of time signal: a two sided spectrum. Only the left half of the spectrum is selected, and the amplitude is multiplied by 2, to account for all the energy in the spectrum.

The FFT gives a two sided energy density spectrum. This is a mathematical consequence of the Fourier Transform. For engineering practice, In this particular situation, only the left hand side of the spectrum is of interest, this is shown in figure A.1.

Bibliography

- [1] Gerard van Oortmerssen. The motions of a ship in shallow water. *Ocean Engineering*, 3(4):221 – 255, 1976. ISSN 0029-8018. doi: [http://dx.doi.org/10.1016/0029-8018\(76\)90025-1](http://dx.doi.org/10.1016/0029-8018(76)90025-1). URL <http://www.sciencedirect.com/science/article/pii/0029801876900251>.
- [2] J.M.J Journée, W.W Massie, and R.H.M. Huijsmans. *Offshore Hydromechanics*. Delft University of Technology, 2015.
- [3] Weoncheol Koo and Jun-Dong Kim. Simplified formulas of heave added mass coefficients at high frequency for various two-dimensional bodies in finite water depth. *International Journal of Naval Architecture and Ocean Engineering*, 7(1):115–127, 2015.
- [4] Onno A.J. Peters and René H.M. Huijsmans. Prediction of relative vertical motion between cargo and htv during offshore loading and discharge. *Proceedings of the ASME 2017 36th International Conference on Ocean, Offshore and Arctic Engineering, OMAE2017, Trondheim, Norway*, 2017.
- [5] M.T. Ruiz, M. Vantorre, T. van Zwijnsvoorde, and G. Delefortrie. Challenges with ship model tests in shallow water waves. *Proceedings of the 12th international Conference on Hydrodynamics, Delft, The Netherlands*, 2016.
- [6] Arjan Voogt. Bilge keel damping from in-field motion measurements. *Report (MARIN's news magazine for the maritime industry)*, (120):14 – 15, 2017.
- [7] Tim Gourlay, Alexander van Greafe, Vladimir Shigunov, and Evert Lataire. Comparison of aqwa, gl rankine, moses, octopus, pdstrip and wamit with model test results for cargo ship wave-induced motions in shallow water. *Proceedings of the ASME 2015 34th International Conference on Ocean, Offshore and Arctic Engineering*, 2015.
- [8] C. Guedes Soares. Effect of spectral shape uncertainty in the short term wave-induced ship responses. *Applied Ocean Research Vol 12*, pages 54–69, 1990.
- [9] Tahsin Tezdogan, Atilla Incecik, and Osman Turan. Full-scale unsteady {RANS} simulations of vertical ship motions in shallow water. *Ocean Engineering*, 123:131 – 145, 2016. ISSN 0029-8018. doi: <https://doi.org/10.1016/j.oceaneng.2016.06.047>. URL <http://www.sciencedirect.com/science/article/pii/S0029801816302372>.
- [10] Z.X. Zhou, Edmond Y.M. Lo, and S.K. Tan. Effect of shallow and narrow water on added mass of cylinders with various cross-sectional shapes. *Ocean Engineering*, 32(10):1199 – 1215, 2005. ISSN 0029-8018. doi: <https://doi.org/10.1016/j.oceaneng.2004.12.001>. URL <http://www.sciencedirect.com/science/article/pii/S0029801805000144>.
- [11] *AQWA-LINE manual, release 12.0*, 2009.
- [12] L.H. Holthuijsen. *Waves in Oceanic and Coastal Waters*. Cambridge University Press, 2007. ISBN 978-0-521-86028-4.
- [13] *AQWA-DRIFT manual, release 12.0*, 2009.
- [14] Berwin A. Turlach. Bandwidth selection in kernel density estimation: A review. *C.O.R.E. and Institut de Statistique, KU Leuven*, 1993.
- [15] Susan Holmes. RMS error, 28-11-2000. <http://statweb.stanford.edu/~susan/courses/s60/split/node60.html> [accessed:08-01-2018].
- [16] Kenneth L. Denman. Spectral analysis: a summary of the theory and techniques. Technical report, Research and Development Directorate Marine Ecology Laboratory Bedford Institute of Oceanography, Dartmouth, Nova Scotia, 1975.

